# Mobile Edge Computing Aided Integrated Sensing and Communication With Short-Packet Transmissions

Ning Huang, Chenglong Dou, *Graduate Student Member, IEEE*, Yuan Wu, *Senior Member, IEEE*, Liping Qian, *Senior Member, IEEE*, Bin Lin, *Senior Member, IEEE*, Haibo Zhou, *Senior Member, IEEE*, and Xuemin Shen, *Fellow, IEEE*

***Abstract*— Integrated sensing and communication (ISAC) provides an emerging paradigm for enabling a variety of next-generation wireless services and applications. Due to the limited computation resources on ISAC devices and the latency as well as the reliability requirements, we propose a paradigm of mobile edge computing (MEC) aided ISAC with short-packet transmissions, where multiple ISAC devices adopt short-packet transmissions to offload their sensed radar data to an edge-server for analysis. We adopt the mutual information to measure the performance of radar sensing and quantify the reliability and latency performances for analyzing the radar-data via edge computing. We formulate an energy minimization problem that jointly optimizes the size of each short packet, the duration of each short packet, the computing-capacity allocations of edge-server, the beamforming of the radar sensing and the offloading transmission, while providing guaranteed performances for the radar sensing, the latency for radar-data analysis, and the reliability of offloading transmission. We identify the hierarchical structure of the formulated problem and divide the problem into three subproblems. For both the bottom-layer problem optimizing the computing-capacity allocations of the edge-server and the middle-layer problem optimizing the size of each short packet and the duration of each short packet, we derive their solutions analytically. Finally, for the top-layer problem optimizing the beamforming of the radar sensing and the offloading transmission, we transform it into a difference of convex (DC) problem which can be efficiently solved. We show the performance advantages of our proposed scheme. The simulation results show that our proposed algorithm can outperform the benchmark algorithms.**

***Index Terms*— Mobile edge computing, integrated sensing and communication, short-packet transmissions.**

Manuscript received 11 February 2023; revised 21 July 2023 and 19 September 2023; accepted 12 December 2023. Date of publication 27 December 2023; date of current version 12 July 2024. This work was supported in part by the National Natural Science Foundation of China under Grant 62122069, Grant 62072490, and Grant 62071431; in part by the Science and Technology Development Fund of Macau, SAR, under Grant 0158/2022/A; in part by the Guangdong Basic and Applied Basic Research Foundation under Grant 2022A1515011287; and in part by the Natural Sciences and Engineering Research Council of Canada under Grant MYRG2020-00107-IOTSC. The associate editor coordinating the review of this article and approving it for publication was M. C. Vuran. *(Corresponding author: Yuan Wu.)*

Ning Huang and Chenglong Dou are with the State Key Laboratory of Internet of Things for Smart City and the Department of Computer and Information Science, University of Macau, Macau, China.

Yuan Wu is with the State Key Laboratory of Internet of Things for Smart City and the Department of Computer and Information Science, University of Macau, Macau, China, and also with the Zhuhai UM Science and Technology Research Institute, Zhuhai 519031, China (e-mail: yuanwu@um.edu.mo).

Liping Qian is with the College of Information Engineering, Zhejiang University of Technology, Hangzhou 310023, China (e-mail: lpqian@zjut.edu.cn).

Bin Lin is with the Department of Communication Engineering, Dalian Maritime University, Dalian 116026, China (e-mail: binlin@dlmu.edu.cn).

Haibo Zhou is with the School of Electronic Science and Engineering, Nanjing University, Nanjing 210093, China (e-mail: haibozhou@nju.edu.cn).

Xuemin Shen is with the Department of Electrical and Computer Engineering, University of Waterloo, Waterloo, ON N2L 3G1, Canada (e-mail: sshen@uwaterloo.ca).

Color versions of one or more figures in this article are available at https://doi.org/10.1109/TWC.2023.3344479.

Digital Object Identifier 10.1109/TWC.2023.3344479

## I. Introduction

INTEGRATED sensing and communication (ISAC), which enables the joint radar sensing and data communications, has been regarded as one of the key paradigms for supporting various emerging wireless services in future 6G networks [1], [2], [3]. Thanks to enabling the dual-functionality of radar sensing and data communications simultaneously, ISAC has been expected to effectively reduce the usage of radio resources (e.g., the frequency channels and time-slots), compared to conventional systems that require separated radio resources to perform radar sensing and data communications. Thus, many researches have been devoted to ISAC with its applications. Despite the potential advantage, the integration of radar sensing and data communications leads to mutual interference between them, which may adversely degrade their respective performances. To address this issue, several studies have focused on optimizing the ISAC performance, e.g., via waveform design [4], [5], [6], [7], [8] and interference mitigation [9], [10].

ISAC devices generate a large volume of sensing data, which can be used for many intelligent applications such as target recognition. Many advanced machine learning and deep learning techniques have been used to improve the analysis accuracy of radar sensing signal, which requires a large amount of computation resources [11], [12]. Due to the limited computation resources on the ISAC devices, locally analyzing the radar-sensing data on the ISAC devices will suffer from a long latency. Mobile edge computing (MEC) [13], [14], [15], [16], [17], [18], [19] provides a promising solution to address this issue. In this work, we consider MEC aided ISAC, in which the ISAC devices offload their sensed radar data to an edge-server for efficient analysis while accounting for the consequent performances, including the radar sensing performance, the latency for the radar-data analysis, and the reliability of offloading transmission.

Although MEC can potentially reduce the latency for analyzing the radar-sensing data, the offloading transmission

of radar-sensing data over wireless links may suffer from the interference from both the radar sensing as well as other ISAC devices' offloading transmissions, which degrades the reliability of the offloading transmission. Such an issue is critical to many fault-sensitive applications and services, in which the radar-sensing data should be delivered to the edge-server in a reliable manner. The short-packet mechanism provides an efficient approach for enabling reliable and low-latency communications [20], [21], [22], [23], [24], [25], [26], in which packets of the short block-length are used for delivering data. In this paper, we investigate the MEC aided ISAC with adaptive short-packet mechanism to reduce the latency and satisfy the reliability requirement. Although many existing studies investigate short-packet transmissions in different networks, little attention has been paid to ISAC which invokes the new performance metric for the radar sensing. Moreover, the existing studies on short-packet transmission usually do not consider the optimization of the sizes of different short packets [20], [21], [22], [23], [24], [25], [26]. Different from the aforementioned works, we consider the paradigm of MEC aided ISAC, where the radar-sensing data is delivered to the edge-server via multiple short packets with optimized packet sizes and transmission duration. Our main contributions are summarized as follows.

- We characterize the mutual influence between the performance of radar sensing and the performance of the sensing-data offloading transmission via short packets. We characterize the decoding error probability of each ISAC device's short packets for its offloading transmission, by accounting for both the interference from all devices' radar sensing as well as other devices' offloading transmissions. We quantify the mutual interference between the radar sensing and the offloading transmission, and future quantify the mutual information from the radar echo as the sensing performance metric.
- We formulate an optimization problem to minimize the system energy consumption and guarantee i) the requirement on the radar-sensing performance, ii) the requirement on the decoding error probability of the ISAC devices' short-packet transmissions (i.e., the reliability requirement), and iii) the requirement on the latency in processing the ISAC devices' sensing-data via MEC (i.e., the latency requirement). To achieve this objective, our problem jointly optimizes the size of each short packet, the duration of each short packet, the computing-capacity allocations of the edge-server, the beamforming for radar sensing, and the beamforming for offloading transmission.
- Despite the non-convexity of the joint optimization problem, we propose an efficient algorithm to compute the solutions. We identify the hierarchical structure of the formulated problem and decompose it into three subproblems, including i) a bottom-layer problem optimizing the computing-capacity allocations of the edge-server, ii) a middle-layer problem optimizing the size of each packet and the duration of each short packet, and iii) a top-layer problem optimizing the beamforming for radar sensing and the beamforming for offloading transmission. For the bottom-layer problem and the middle-layer problem, we derive their optimal solutions analytically. For the top-layer problem, we transform it into a difference of convex (DC) problem which can thus be efficiently solved.
- Extensive numerical results are provided to validate the performance advantage of our proposed scheme and the effectiveness of the proposed algorithm. We show the performance advantage of our proposed algorithm in comparison with two different benchmark algorithms. The simulation results show that our proposed algorithm can outperform the benchmark algorithms.

The remainder of this paper is organized as follows. We review the related studies in Section II. We formulate a joint optimization problem in Section III and further propose an efficient algorithm for solving the problem in Section V. Numerical results are presented in Section VI. We finally conclude this work in Section VII and discuss the future directions.

## II. Related Studies

There exists a coupling effect between the radar sensing and data communications due to sharing the same radio resources in ISAC. The integration of two functionalities incurs mutual interference which degrades both the performances of radar sensing and communication. Several studies have been devoted to addressing the mutual interference via waveform design. Liu et al. in [4] utilized the Cramér-Rao bound to measure the radar sensing performance and minimized the Cramér-Rao bound meanwhile satisfying the signal noise ratio constraint of the communication devices. The authors in [5] proposed a single-tratget-multi-beams radar beam alignment scheme to allocate multiple radar beams to the target, which can obtain more accurate information on estimated ranges and velocities. Ni et al. in [6] studied the optimal waveform design in communication-centric ISAC system, under the constraint of multi-metrics including the signal to interference plus noise ratio (SINR), the mutual information and the Cramér-Rao bound. Yuan et al. in [7] investigated the orthogonal time frequency space modulation for ISAC in vehicular networks. Different interference mitigation schemes have also been proposed for ISAC. Chen et al. in [9] studied the full-duplex self-interference cancellation in dual-functional radar-communication system, aiming to maximize the radar SINR meanwhile satisfying the requirement of communication throughput. Zhang et al. in [10] utilized intelligent reflecting surface to suppress the interference between the radar sensing and communication for ISAC in cloud radio access network.

Different from the above mentioned works, we consider that the ISAC devices have limited computation-resources and cannot perform a timely local processing (i.e., analysis) of the radar-sensing data. Thus, we propose a paradigm of MEC aided ISAC. MEC has been regarded as a promising paradigm for enabling the computation-intensive yet latency-sensitive services in wireless networks. Thanks to its potentials, many studies have investigated the performance optimizations for different MEC aided paradigms, e.g., unmanned aerial vehicle (UAV) assisted network [15], [16], vehicular networks [17], space-air-ground integrated networks [18]. Recently, there have been several studies leveraging ISAC for MEC. Liu et al. in [27] investigated the sensing data offloading in the UAV assisted networks and proposed an energy-efficient strategy

for computation offloading. However, the radar-sensing performance has not been accounted for in [27]. The authors in [28] utilized IRS to improve both the radar sensing and data offloading performances in ISAC assisted MEC network, in which the radar-sensing data is not related to the offloading transmission. Different from [28], we consider that the radar-sensing data generated by the ISAC devices is offloaded to the edge-server for analysis.

There have been several studies investigating the short-packet transmission. Li et al. in [21] investigated the physical layer security aided secure short-packet transmissions for the ultra-reliable and low-latency communication. Pan et al. in [22] jointly optimized the block-length of the short packet and the UAV's allocation in UAV networks. Cai et al. in [23] investigated the resource allocation in a two-way UAV relaying communication with the short-packet mechanism, with the objective of maximizing the transmission throughput under both the latency and reliability requirements. Zhou et al. in [24] investigated the short packet transmissions in the mobile edge computing assisted radio access network. Ren et al. in [25] investigated multiple input multiple output (MIMO) enhanced short-packet transmissions in industrial Internet of Things and maximized the achievable data rate by optimizing the pilot and payload transmission power. The authors in [26] analyzed the control and non-payload communication link in UAV networks for the ultra-reliable and low-latency communication. Different from the existing works, we consider the MEC aided ISAC with short-packet transmissions, where the radar-sensing data is reliably delivered to the edge-server via multiple short packets, with the guaranteed performances of radar sensing, offloading latency and the decoding error probability of the packets.

## III. System Model and Problem Formulation

As shown in Figure 1, we consider the MEC aided ISAC, which includes a group of $\mathcal{K} = \{1, 2, \ldots, K\}$ ISAC devices and one wireless access point (AP). The wireless AP is equipped with one antenna and is connected to an edge-server. Each ISAC device is equipped with $M$ antennas. We consider a general spectrum sharing approach, i.e., all ISAC devices conduct the radar sensing and data transmissions simultaneously over the same frequency channel. Although the spectrum sharing can reduce the usage of bandwidth, it incurs complicated co-channel interference which will be modeled in Section III-B and Section III-C.

As illustrated before, each ISAC device offloads its radar-sensing data to the edge-server for analysis with the short-packet transmission. To model the offloading transmission, we consider that the time-horizon is divided into $N$ time-slots with the length of each time-slot denoted by $\tau$. Each time-slot is used for sending one short packet (containing the radar-sensing data) to the edge-server from the ISAC devices. Thus, $\tau$ also denotes the duration of each short packet. In our problem formulation, we will treat $\tau$ as a decision variable, which is equivalent to optimize the latency of the offloading transmission. In this work, we consider that the channel power gains vary across different time-slots. To adapt to the time-varying channels for different ISAC devices, we optimize their packet sizes at different time-slots during the offloading transmissions.

### A. Offloading Transmissions via Short Packets

According to the practical radar detection [29], the total number of bits of the radar-sensing data generated by the $k$-th ISAC device can be modeled as

$$D_k = \rho \delta_k \xi_\theta \varsigma_k \iota_k, \tag{1}$$

where $\rho$ is a parameter depending on the sampling configuration. Parameter $\delta_k$ denotes the switching speed of the radar beam. $\xi_\theta$ is the quantization coefficient for the angles, and $\varsigma_k$ is the number of quantization bits for each sample. In addition, parameter $\iota_k \geq 1$ is a constant determined by the data redundancy.

Recall that the time-horizon is divided into a sequence of $\mathcal{N} = \{1, 2, \ldots, N\}$ time-slots. A time-slot is used to send each ISAC device's one short packet to the edge-server, and $D_k$ denotes the size of the total radar-sensing data of ISAC device $k$. We use $d_{kn}$ to denote the size of the $n$-th short packet at the $n$-th time-slot sent by ISAC device $k$. Thus, to complete sending device $k$'s total data $D_k$, the following equation should hold[1]:

$$\sum_{n \in \mathcal{N}} d_{kn} = D_k, \ \forall k \in \mathcal{K}. \tag{2}$$

To quantify the reliability of the offloading transmission, we use $\varepsilon_{kn}$ to denote the decoding error probability for device $k$'s $n$-th short packet (i.e., at the $n$-th time-slot). It is noticed that conventional Shannon channel capacity cannot be directly used for modeling the short-packet transmission. Accounting for the feature of the finite block-length, the maximum achievable throughput from ISAC device $k$ to the edge-sever at the $n$-th time-slot can be expressed as [30]

$$R_{kn} = B\left(\log_2(1+\gamma_{kn}^{\text{off}}) - \sqrt{\frac{V_{kn}}{B\tau}}\, Q^{-1}(\varepsilon_{kn})\right), \tag{3}$$

where $B$ denotes the channel bandwidth. Variable $\gamma_{kn}^{\text{off}}$ denotes the SINR for the $k$-th ISAC device's offloading transmission at the $n$-th time-slot, which will be quantified in Section III-B. As mentioned before, $\tau$ is the transmission duration of each packet. $Q^{-1}(\cdot)$ is the inverse of Q-function, i.e., $Q(x) = \frac{1}{\sqrt{2\pi}} \int_x^\infty e^{-\frac{y^2}{2}} dy$. In eq. (3), $V_{kn}$ denotes the channel dispersion which can be expressed as

$$V_{kn} = \frac{1}{(\ln 2)^2}\left(1 - \frac{1}{(1+\gamma_{kn}^{\text{off}})^2}\right). \tag{4}$$

When sending a short packet of $d_{kn}$ bits with duration $\tau$, the following equation should hold:

$$R_{kn}\tau = d_{kn}. \tag{5}$$

By substituting eq. (3) into eq. (5), we can obtain ISAC device $k$'s decoding error probability at time-slot $n$ as

$$\varepsilon_{kn} = Q\left(\sqrt{\frac{B\tau}{V_{kn}}}\log_2(1+\gamma_{kn}^{\text{off}}) - \frac{d_{kn}}{\sqrt{B\tau V_{kn}}}\right). \tag{6}$$

[1]In this paper, similar to the paradigm of partial computation offloading in MEC [15], we assume that the volume of the radar-sensing data can be divided into multiple pieces.

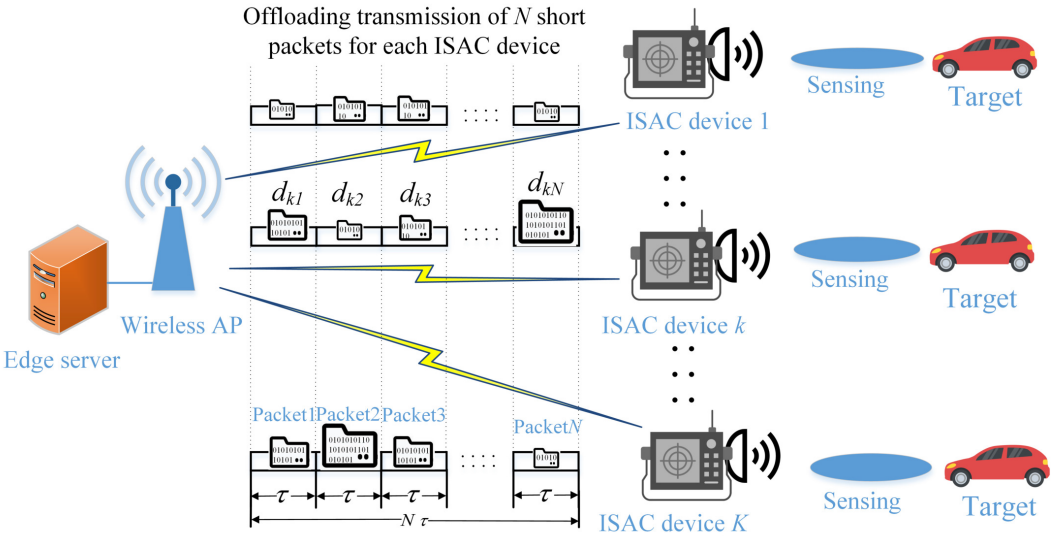


Fig. 1. MEC aided ISAC with short-packet transmissions: a group of $K$ ISAC devices perform the radar sensing and offloading transmissions simultaneously over the same channel.

Based on eq. (6), we can express the overall decoding error probability for ISAC device $k$, which is denoted by $\varepsilon_k$, as

$$\varepsilon_k = \sum_{n=1}^{N} \varepsilon_{kn} \Big( \prod_{j=1}^{n-1} (1-\varepsilon_{kj}) \Big). \tag{7}$$

Since the values of $\{\epsilon_{kn}\}$ are usually very small (e.g., $1 \times 10^{-5}$) for reaching the requirement of ultra-reliable transmission, similar to the approximation in [31], we can approximate $\epsilon_k$ by neglecting the series of production terms such as $\epsilon_{k1}\epsilon_{k2}\epsilon_{k3}$ in eq. (7), which leads to

$$\varepsilon_k \approx \sum_{n=1}^{N} \varepsilon_{kn}. \tag{8}$$

To ensure the reliability of ISAC device $k$'s offloading transmission, we impose the following constraint:

$$\varepsilon_k \leq \varepsilon_k^{\max}, \ \forall k \in \mathcal{K}, \tag{9}$$

where $\varepsilon_k^{\max}$ denotes the maximum of the decoding error probability of ISAC device $k$.

### B. SINR Analysis for the Offloading Transmission

In eq. (6), we need to provide $\gamma_{kn}^{\text{off}}$ to evaluate the decoding error probability. We thus quantify $\gamma_{kn}^{\text{off}}$ in this subsection by accounting for the mutual interference between the radar sensing and the devices' offloading transmissions. The details are as follows. To increasing the degrees of freedom of MIMO radar waveform, we utilize both the precoded individual communication and radar waveforms [32]. As a result, the transmitted signal is the sum of the precoded communication and radar waveforms. For the $k$-th ISAC device at the $n$-th time-slot, we use $\mathbf{s}_{kn}^{\text{rad}} \in \mathbb{C}^{M\times 1}$ to denote the vector of $M$ radar waveforms and use $\mathbf{W}_{kn}^{\text{rad}} \in \mathbb{C}^{M\times M}$ to denote the precoding matrix (i.e., beamforming) for the corresponding radar waveforms. We use $\mathbf{s}_{kn}^{\text{off}} \in \mathbb{C}^{M\times 1}$ to denote the vector of $M$ parallel communication symbols which are offloaded to the edge-server, and we use $\mathbf{W}_{kn}^{\text{off}} \in \mathbb{C}^{M\times M}$ to denote the precoding matrix for the offloading transmission. The transmitted signal of the $k$-th ISAC device at the $n$-th time-slot can be expressed as

$$\mathbf{x}_{kn} = \mathbf{W}_{kn}^{\text{rad}} \mathbf{s}_{kn}^{\text{rad}} + \mathbf{W}_{kn}^{\text{off}} \mathbf{s}_{kn}^{\text{off}}, \tag{10}$$

The received signal of the AP at the $n$-th time-slot can be expressed as

$$y_n = \sum_{k\in\mathcal{K}} (\mathbf{h}_{kn})^H \mathbf{x}_{kn} + \upsilon_n, \tag{11}$$

where $\mathbf{h}_{kn} \in \mathbb{C}^{M\times 1}$ denotes the communication channel matrix from the $k$-th ISAC device to the edge-server, and $\upsilon_n$ denotes the additive white Gaussian noise with covariance $\sigma^2$.

By substituting the expression of $\mathbf{x}_{kn}$ (i.e., eq. (10)) into eq. (11), the received signal of the $k$-th ISAC device at the $n$-th time-slot can be expressed as

$$y_{kn}^{\text{off}} = \underbrace{(\mathbf{h}_{kn})^H \mathbf{W}_{kn}^{\text{off}} \mathbf{s}_{kn}^{\text{off}}}_{\text{desired offloading signal}} + \underbrace{\sum_{j\neq k, j\in\mathcal{K}} (\mathbf{h}_{jn})^H \mathbf{W}_{jn}^{\text{off}} \mathbf{s}_{jn}^{\text{off}}}_{\text{interference from other devices' offloading signal}} + \underbrace{\sum_{k\in\mathcal{K}} (\mathbf{h}_{kn})^H \mathbf{W}_{kn}^{\text{rad}} \mathbf{s}_{kn}^{\text{rad}}}_{\text{interference from all devices' radar signal}} + \upsilon_n. \tag{12}$$

With eq. (12), the SINR $\gamma_{kn}^{\text{off}}$ for the $k$-th device's offloading transmission at the $n$-th time-slot can be expressed as

$$\gamma_{kn}^{\text{off}} = \frac{||(\mathbf{h}_{kn})^H \mathbf{W}_{kn}^{\text{off}}||^2}{\sum\limits_{k\in\mathcal{K}} ||(\mathbf{h}_{kn})^H \mathbf{W}_{kn}^{\text{rad}}||^2 + \sum\limits_{j\neq k, j\in\mathcal{K}} ||(\mathbf{h}_{jn})^H \mathbf{W}_{jn}^{\text{off}}||^2 + \sigma^2}. \tag{13}$$

### C. Modeling of Radar Sensing

We quantify the mutual information to measure the radar sensing performance, which provides an effective measure for

the amount of the information of the target captured by the radar echo signal [33], [34], [35]. The received radar signal of the $k$-th ISAC device at the $n$-th time-slot can be written as

$$\mathbf{y}_{kn}^{\mathrm{rad}}=\mathbf{A}_{kn}\mathbf{x}_{kn}+\sum_{j\neq k,j\in\mathcal{K}}\bar{\mathbf{H}}_{kjn}\mathbf{x}_{jn}+\mathbf{v}_{kn}, \tag{14}$$

where $\mathbf{A}_{kn}\in\mathbb{C}^{M\times M}$ is the target response matrix between the $k$-th ISAC device and its target at the $n$-th time-slot. $\mathbf{A}_{kn}$ can be modeled as $\mathbf{A}_{kn}=\bar{\beta}_{kn}\mathbf{a}_{kn}^{\mathrm{rec}}(\mathbf{a}_{kn}^{\mathrm{tran}})^H$, where $\bar{\beta}_{kn}$ denotes the complex path loss. $\mathbf{a}_{kn}^{\mathrm{tran}}$ and $\mathbf{a}_{kn}^{\mathrm{rec}}$ denote the array steering vectors of the transmitter and receiver, respectively. $\bar{\mathbf{H}}_{kjn}\in\mathbb{C}^{M\times M}$ denotes the interference channel matrix from the $k$-th device to the $j$-th device at the $n$-th time-slot. $\mathbf{v}_{kn}$ is the receiver noise of the $k$-th device at the $n$-th time-slot with variance $\sigma^2$.

By substituting the expression of $\mathbf{x}_{kn}$ (i.e., eq. (10)) into eq. (14), the received radar signal can be written as

$$\begin{aligned}\mathbf{y}_{kn}^{\mathrm{rad}}=&\underbrace{\mathbf{A}_{kn}\mathbf{W}_{kn}^{\mathrm{rad}}\mathbf{s}_{kn}^{\mathrm{rad}}}_{\text{desired radar signal}}+\underbrace{\sum_{j\neq k,j\in\mathcal{K}}\bar{\mathbf{H}}_{jkn}\mathbf{W}_{jn}^{\mathrm{rad}}\mathbf{s}_{jn}^{\mathrm{rad}}}_{\text{interference from other devices' radar signal}}\\&\underbrace{+\mathbf{A}_{kn}\mathbf{W}_{kn}^{\mathrm{off}}\mathbf{s}_{kn}^{\mathrm{off}}+\sum_{j\neq k,j\in\mathcal{K}}\bar{\mathbf{H}}_{jkn}\mathbf{W}_{jn}^{\mathrm{off}}\mathbf{s}_{jn}^{\mathrm{off}}}_{\text{interference from all devices' offloading signal}}+\mathbf{v}_{kn}.\end{aligned} \tag{15}$$

We use $\mathbf{R}_{kn}^{\mathrm{x}}$ to denote the covariance of the transmitted waveform, i.e.,

$$\begin{aligned}\mathbf{R}_{kn}^{\mathrm{x}}&=\mathbb{E}(\mathbf{x}_{kn}\mathbf{x}_{kn}^H)=\mathbf{W}_{kn}^{\mathrm{rad}}(\mathbf{W}_{kn}^{\mathrm{rad}})^H+\mathbf{W}_{kn}^{\mathrm{off}}(\mathbf{W}_{kn}^{\mathrm{off}})^H\\&=\mathbf{R}_{kn}^{\mathrm{rad}}+\mathbf{R}_{kn}^{\mathrm{off}},\end{aligned} \tag{16}$$

where $\mathbf{R}_{kn}^{\mathrm{rad}}$ denotes the covariance of its radar waveform, i.e.,

$$\mathbf{R}_{kn}^{\mathrm{rad}}=\mathbf{W}_{kn}^{\mathrm{rad}}(\mathbf{W}_{kn}^{\mathrm{rad}})^H, \tag{17}$$

and $\mathbf{R}_{kn}^{\mathrm{off}}$ denotes the covariance of its communication waveform, i.e.,

$$\mathbf{R}_{kn}^{\mathrm{off}}=\mathbf{W}_{kn}^{\mathrm{off}}(\mathbf{W}_{kn}^{\mathrm{off}})^H. \tag{18}$$

Based on the expression of the received radar signal in eq. (15), the mutual information for radar sensing between the $k$-th ISAC device and its target at the $n$-th time-slot can be expressed as

$$I_{kn}^{\mathrm{rad}}=B\log\det\left(\mathbf{I}_M+\mathbf{A}_{kn}\mathbf{R}_{kn}^{\mathrm{rad}}\mathbf{A}_{kn}^H\mathbf{\Phi}_{kn}^{-1}\right), \tag{19}$$

where $\det(\cdot)$ denotes the determinant of a matrix, and $\mathbf{I}_M$ denotes an identity matrix with the dimension $M\times M$. In eq. (19), $\mathbf{\Phi}_{kn}$ is given by

$$\begin{aligned}\mathbf{\Phi}_{kn}=&\sum_{j\neq k,j\in\mathcal{K}}\bar{\mathbf{H}}_{jkn}\mathbf{R}_{jn}^{\mathrm{rad}}(\bar{\mathbf{H}}_{jkn})^H+\sum_{j\in\mathcal{K}}\mathbf{C}_{jkn}\mathbf{R}_{jn}^{\mathrm{off}}(\mathbf{C}_{jkn})^H\\&+\sigma^2\mathbf{I}_M,\end{aligned} \tag{20}$$

where

$$\mathbf{C}_{jkn}=\begin{cases}\mathbf{A}_{kn},\ j=k,\\ \bar{\mathbf{H}}_{jkn},\ j\neq k.\end{cases}$$

### D. Latency for Radar-Sensing Data Analysis

To quantify the latency for analyzing each ISAC device's radar-sensing data via MEC, we account for both the latency of each device's offloading transmission and the latency of performing the analysis at the edge-server for each device. The details are as follows.

- For each ISAC device, its offloading transmission duration can be expressed $N\tau$, where $N$ is the fixed parameter denoting the number of the time-slots and $\tau$ denotes the length of each time-slot (notice that we will optimize $\tau$ in our following problem formulation). As shown in Figure 1, for the sake of clear modeling, we assume that all ISAC devices use the same offloading transmission duration, i.e., $N\tau$. The reason can be explained as follows. If we allow different ISAC devices to use different offloading transmission durations, then the interference items in eq. (12) and eq. (15) will become very complicated. Specifically, the interference items depend on which subset of the ISAC devices are performing offloading transmissions simultaneously. As a result, it becomes very complicated to model $\gamma_{kn}^{\mathrm{off}}$ and $I_{kn}^{\mathrm{rad}}$ unless we know the ordering of the ISAC devices when they complete their offloading transmissions. Due to the above reason, we assume that all ISAC devices use the same offloading transmission duration, i.e., $N\tau$.
- After the edge-server receives the radar-sensing data from the ISAC devices, the edge-server processes and analyzes the data by using the correspondingly allocated computing-capacities to different devices. We use $f_k$ to denote the computing-capacity allocated to ISAC device $k$. The latency for the edge-server to complete processing all ISAC devices' radar-sensing data can be given by

$$t^{\mathrm{server}}=\max_{k\in\mathcal{K}}\{\frac{\zeta D_k}{f_k}\}, \tag{21}$$

where $\zeta$ is a coefficient representing the number of CPU cycles to process one bit data.

Based on the above analysis, the overall system-latency can be expressed as[2]

$$T^{\mathrm{ove}}=N\tau+t^{\mathrm{server}}=N\tau+\max_{k\in\mathcal{K}}\{\frac{\zeta D_k}{f_k}\}. \tag{22}$$

### E. Modeling of the Energy Consumption

The overall energy consumption includes two parts, i.e., the energy consumption of all ISAC devices and the energy consumption of the edge-server. We quantify these two parts as follows.

- Each ISAC device's energy consumption includes two parts, i.e., the energy consumption for radar sensing and the energy consumption for its offloading transmission.

[2]In this work, for the sake of clear modeling, we assume that the sensed radar data is sent to the edge-server immediately when it is obtained, i.e., there is no processing latency at the ISAC devices.

Thus, from all ISAC devices' perspective, the total energy consumption can be expressed as

$$\sum_{k\in\mathcal{K}} E_k^{\text{device}} = \sum_{n\in\mathcal{N}}\sum_{k\in\mathcal{K}} \tau \text{Tr}\big(\mathbf{W}_{kn}^{\text{rad}}(\mathbf{W}_{kn}^{\text{rad}})^H + \mathbf{W}_{kn}^{\text{off}}(\mathbf{W}_{kn}^{\text{off}})^H\big). \quad (23)$$

In eq. (23), with different beamformings $\mathbf{W}_{kn}^{\text{off}}$ and $\mathbf{W}_{kn}^{\text{rad}}$, ISAC device $k$'s transmit-power at time-slot $n$ varies. Thus, optimizing beamformings $\mathbf{W}_{kn}^{\text{off}}$ and $\mathbf{W}_{kn}^{\text{rad}}$ can adjust ISAC device $k$'s transmit-powers for radar sensing and offloading transmission, respectively.

- The edge-server consumes energy to process the radar-sensing data from the ISAC devices. The corresponding power consumption per second can be expressed as $\kappa f_k^3$ [36], where $\kappa$ represents the energy-efficiency coefficient depending on the architecture of the CPU. Since processing $D_k$ bits requires a latency of $\frac{\zeta D_k}{f_k}$, the energy consumption to process $D_k$ bits data from the $k$-th ISAC device is $\zeta D_k \kappa f_k^2$. Thus, the energy consumption of the edge-server to process all ISAC devices' sensing data can be expressed as

$$E^{\text{server}} = \sum_{k\in\mathcal{K}} \kappa\zeta D_k f_k^2. \quad (24)$$

Based on the above analysis, the overall system energy consumption can be expressed as

$$E^{\text{ove}} = \varpi_1 \sum_{k\in\mathcal{K}} E_k^{\text{device}} + \varpi_2 E^{\text{server}}, \quad (25)$$

where $\varpi_1$ and $\varpi_2$ are the weights for the ISAC devices and the edge-server, respectively.

In addition, from each individual ISAC device's perspective, its transmit-power for both radar-sensing and offloading transmission should be no greater than its transmit-power capacity. i.e.,

$$\text{Tr}\big(\mathbf{W}_{kn}^{\text{rad}}(\mathbf{W}_{kn}^{\text{rad}})^H + \mathbf{W}_{kn}^{\text{off}}(\mathbf{W}_{kn}^{\text{off}})^H\big) \le P_k^{\max}, \forall k\in\mathcal{K}, \forall n\in\mathcal{N}, \quad (26)$$

where $P_k^{\max}$ is the maximum transmit-power of the $k$-th ISAC device. In eq. (26), $\text{Tr}(\cdot)$ denotes the trace of a matrix.

### F. Problem Formulation

We formulate the following overall energy consumption minimization problem (OEM) (here, 'OEM' stands for the 'overall energy consumption minimization'). Constraint (27) ensures that the overall latency cannot exceed the system latency limit which is denoted as $T^{\max}$. Constraint (28) ensures that the mutual information of radar sensing should satisfy the mutual information requirement $I_{kn}^{\min}$. Constraint (29) ensures that the total computing-capacities allocated to all ISAC devices cannot exceed the edge-server's computing-capacity which is denoted as $F^{\text{total}}$. Constraint (9) ensures that the decoding error probability for each ISAC device $\varepsilon_k$ cannot exceed the decoding error probability limit $\varepsilon_k^{\max}$. Constraint (26) is the transmit-power constraint for each ISAC device.

$$\begin{aligned}
\text{(OEM):}\quad & \min\ E^{\text{ove}} \\
\text{subject to:}\quad & T^{\text{ove}} \le T^{\max}, && (27)\\
& I_{kn}^{\text{rad}} \ge I_{kn}^{\min},\ \forall k\in\mathcal{K},\ \forall n\in\mathcal{N}, && (28)\\
& \sum_{k\in\mathcal{K}} f_k \le F^{\text{total}}, && (29)\\
& \text{constraints: (2), (9), (26),} \\
\text{variables:}\quad & \{\mathbf{W}_{kn}^{\text{off}}\}, \{\mathbf{W}_{kn}^{\text{rad}}\}, \{f_k\}, \\
& \tau, \{d_{kn}\}.
\end{aligned}$$

In Problem (OEM), we aim to efficiently exploit the sensing, communication and computation resources to enhance the cooperation and balance the trade-off among the radar sensing, short-packet transmission and MEC. Problem (OEM) is a complicated non-convex optimization problem, which is challenging to solve efficiently. In the next section, we propose a layered algorithm for solving Problem (OEM).

## IV. Hierarchical Structure of Problem (OEM) and Proposed Algorithm

### A. Hierarchical Structure of Problem (OEM)

We exploit the hierarchical structure of Problem (OEM) for efficiently solving it. The details are as follows.

*Bottom-layer problem to optimize $\{f_k\}$ under given $\{\mathbf{W}_{kn}^{\text{off}}\}$, $\{\mathbf{W}_{kn}^{\text{rad}}\}$, $\tau$ and $\{d_{kn}\}$.* We firstly consider that the beamforming for radar sensing $\{\mathbf{W}_{kn}^{\text{rad}}\}$, the beamforming for offloading transmission $\{\mathbf{W}_{kn}^{\text{off}}\}$, the duration of each short packet $\tau$ and the size of each short packet $\{d_{kn}\}$ are given. Then, we optimize the computing-capacity allocations $\{f_k\}$ of the edge-server. This leads to the bottom-layer Problem (OEM-BOT) as follows.

$$\begin{aligned}
\text{(OEM-BOT):}\quad & E^{\text{BOT}}\big(\{\mathbf{W}_{kn}^{\text{off}}\}, \{\mathbf{W}_{kn}^{\text{rad}}\}, \tau, \{d_{kn}\}\big) \\
& = \min\ E^{\text{ove}} \\
\text{subject to:}\quad & \text{constraints: (27), (29),} \\
\text{variables:}\quad & \{f_k\}.
\end{aligned}$$

*Middle-layer problem to optimize $\tau$ and $\{d_{kn}\}$ under given $\{\mathbf{W}_{kn}^{\text{off}}\}$ and $\{\mathbf{W}_{kn}^{\text{rad}}\}$.* With the optimal value of $E^{\text{BOT}}(\{\mathbf{W}_{kn}^{\text{off}}\}, \{\mathbf{W}_{kn}^{\text{rad}}\}, \tau, \{d_{kn}\})$ by solving Problem (OEM-BOT), we then continue to optimize the duration of each short packet $\tau$, and the sizes of different devices' short packets at different time-slots $\{d_{kn}\}$. This leads to the middle-layer Problem (OEM-MID) as follows.

$$\begin{aligned}
\text{(OEM-MID):}\quad & E^{\text{MID}}\big(\{\mathbf{W}_{kn}^{\text{off}}\}, \{\mathbf{W}_{kn}^{\text{rad}}\}\big) \\
& = \min\ E^{\text{BOT}}\big(\{\mathbf{W}_{kn}^{\text{off}}\}, \{\mathbf{W}_{kn}^{\text{rad}}\}, \tau, \{d_{kn}\}\big) \\
\text{subject to:}\quad & \text{constraints: (9), (30),} \\
\text{variables:}\quad & \tau, \{d_{kn}\}.
\end{aligned}$$

We will illustrate soon that constraint (30) comes from some manipulations of constraint (29).

*Top-layer problem to optimize $\{\mathbf{W}_{kn}^{\text{off}}\}$ and $\{\mathbf{W}_{kn}^{\text{rad}}\}$.* After obtaining $E^{\text{MID}}(\{\mathbf{W}_{kn}^{\text{off}}\}, \{\mathbf{W}_{kn}^{\text{rad}}\})$ by solving Problem (OEM-MID), we continue to optimize the beamforming for radar sensing $\{\mathbf{W}_{kn}^{\text{rad}}\}$ and the beamforming for offloading

transmission $\{\mathbf{W}_{kn}^{\text{off}}\}$. This leads to the top-layer Problem (OEM-TOP) as follows.

$$\begin{aligned}\text{(OEM-TOP):}\quad &\min\ E^{\text{MID}}\big(\{\mathbf{W}_{kn}^{\text{off}}\},\{\mathbf{W}_{kn}^{\text{rad}}\}\big)\\ \text{subject to:}\quad &\text{constraints: (26), (28), (30),}\\ \text{variables:}\quad &\{\mathbf{W}_{kn}^{\text{off}}\},\{\mathbf{W}_{kn}^{\text{rad}}\}.\end{aligned}$$

Figure 2 shows the above discussed hierarchical structure of Problem (OEM). The reason for using the above hierarchical structure to solve Problem (OEM) can be justified as follows. Exploiting the feature of Problem (OEM-BOT), we can derive its analytical solution (i.e., Proposition 1). Based on the optimal solution of Problem (OEM-BOT), we can derive the analytical solution of Problem (OEM-MID) (i.e., Proposition 2 and Proposition 3), followed by the objective function of Problem (OEM-TOP). Problem (OEM-TOP) can then be transformed into a DC problem for computing its solution.

### B. Analytical Solution for Problem (OEM-BOT)

*Proposition 1:* Problem (OEM-BOT) is feasible, if the given value of $\tau$ satisfies

$$\tau \le \frac{T^{\max}}{N}-\frac{\zeta}{NF^{\text{total}}}\sum_{k\in\mathcal{K}} D_k. \tag{30}$$

Moreover, with the given value of $\tau$ satisfying eq. (30), the optimal solutions of $\{f_k\}$ for Problem (OEM-BOT) can be expressed as

$$f_k^* = \frac{\zeta D_k}{T^{\max}-N\tau}, \forall k\in\mathcal{K}. \tag{31}$$

*Proof:* Please refer to Appendix A. ∎

As illustrated in the proof of Proposition 1, constraint (30) comes from constraint (29) after some mathematical manipulations. Constraint (30) is used in Problem (OME-MID) to guarantee that the given value of $\tau$ can ensure Problem (OEM-BOT) to be feasible.

### C. Analytical Solution for Problem (OEM-MID)

By substituting the optimal solution of $\{f_k\}$ for Problem (OEM-BOT) (i.e., eq. (31) in Proposition 1) into the objective function of Problem (OEM-MID), we can transform the objective function of Problem (OEM-MID) into

$$\varpi_1\tau\hat{u}+\varpi_2\kappa\zeta^3\sum_{k\in\mathcal{K}}\frac{D_k^3}{(T^{\max}-N\tau)^2}, \tag{32}$$

where $\hat{u}$ can be given by

$$\hat{u}=\sum_{n\in\mathcal{N}}\sum_{k\in\mathcal{K}}\text{Tr}\big(\mathbf{W}_{kn}^{\text{rad}}(\mathbf{W}_{kn}^{\text{rad}})^H+\mathbf{W}_{kn}^{\text{off}}(\mathbf{W}_{kn}^{\text{off}})^H\big). \tag{33}$$

For the sake of clear presentation, we use "$\hat{}$" to denote the variables whose values are given under the given values of $\mathbf{W}_{kn}^{\text{rad}}$ and $\mathbf{W}_{kn}^{\text{off}}$.

The most difficult part in Problem (OEM-MID) comes from constraint (9) (i.e., $\varepsilon_k=\sum_{n\in\mathcal{N}}\varepsilon_{kn}\le\varepsilon_k^{\max}$). We firstly identify its monotonic property in Lemma 1 below.

*Lemma 1:* In constraint (9), $\varepsilon_{kn}$ is monotonically decreasing with $\tau$, which means that $\varepsilon_k$ is monotonically decreasing with $\tau$.

*Proof:* Please refer to Appendix B. ∎

We introduce a series of variables $\{\hat{\tau}_k\}$ as follows:

$$\varepsilon_k\big(\hat{\tau}_k,\{d_{kn}\}\big)=\sum_{n\in\mathcal{N}}\varepsilon_{kn}(\hat{\tau}_k,d_{kn})=\varepsilon_k^{\max},\ \forall k\in\mathcal{K}, \tag{34}$$

where $\varepsilon_k$ and $\varepsilon_{kn}$ are the functions of $\hat{\tau}_k$ and $\{d_{kn}\}$ as shown in eq. (8) and eq. (6), respectively. Then, the optimal solution of $\tau$ is given by Proposition 2 below.

*Proposition 2:* Problem (OEM-MID) is feasible, if the given values of $\{\mathbf{W}_{kn}^{\text{off}}\}$ and $\{\mathbf{W}_{kn}^{\text{rad}}\}$ satisfy

$$\hat{\tau}_k \le \frac{T^{\max}}{N}-\frac{\zeta}{NF^{\text{total}}}\sum_{k\in\mathcal{K}} D_k,\ \forall k\in\mathcal{K}, \tag{35}$$

where $\hat{\tau}_k$ is the function of $\{\mathbf{W}_{kn}^{\text{off}}\}$ and $\{\mathbf{W}_{kn}^{\text{rad}}\}$ as illustrated later in eq. (39) (Both $\{\mathbf{W}_{kn}^{\text{off}}\}$ and $\{\mathbf{W}_{kn}^{\text{rad}}\}$ are contained in $\gamma_{kn}^{\text{off}}$ in eq. (39)).

Under the given values of $\{\mathbf{W}_{kn}^{\text{off}}\}$ and $\{\mathbf{W}_{kn}^{\text{rad}}\}$ satisfying eq. (35), the optimal solution of $\tau$ for Problem (OEM-MID) can be expressed as

$$\tau^*=\max_{k\in\mathcal{K}}\{\hat{\tau}_k\}, \tag{36}$$

where the expressions of $\{\hat{\tau}_k\}$ are derived later in Proposition 3.

*Proof:* Please refer to Appendix C. ∎

As illustrated later, constraint (35) is used as a constraint of Problem (OEM-TOP). Since the values of $\{\mathbf{W}_{kn}^{\text{off}}\}$ and $\{\mathbf{W}_{kn}^{\text{rad}}\}$ in Problem (OEM-TOP) always satisfy constraint (35), the given values of $\{\mathbf{W}_{kn}^{\text{off}}\}$ and $\{\mathbf{W}_{kn}^{\text{rad}}\}$ in Problem (OEM-MID) can ensure Problem (OEM-MID) to be feasible.

The key of Proposition 2 is to determine the values of $\{\hat{\tau}_k\}$, with each $\hat{\tau}_k$ coupled with $\{d_{kn}\}_{\mathcal{N}}$ according to eq. (34). We firstly give the condition for the optimal solutions of $\{d_{kn}\}$ in Lemma 2 below.

*Lemma 2:* For each ISAC device $k$, its optimal solutions of $\{d_{kn}\}_{n\in\mathcal{N}}$ satisfy the following condition:

$$\varepsilon_{k1}(\hat{\tau}_k,d_{k1}^*)=\varepsilon_{k2}(\hat{\tau}_k,d_{k2}^*)=\ldots=\varepsilon_{kN}(\hat{\tau}_k,d_{kN}^*)=\frac{\varepsilon_k^{\max}}{N},\quad \forall k\in\mathcal{K}. \tag{37}$$

*Proof:* Please refer to Appendix D. ∎

With Lemma 2, we can derive the optimal solutions of $\{d_{kn}\}$ and the values of $\{\hat{\tau}_k\}$ in Proposition 3.

*Proposition 3:* For each ISAC device $k$, its optimal packet sizes at different time-slots can be expressed as

$$d_{kn}^*=B\hat{\tau}_k\log_2(1+\gamma_{kn}^{\text{off}})-\sqrt{B\hat{\tau}_kV_{kn}}Q^{-1}\Big(\frac{\varepsilon_k^{\max}}{N}\Big),\quad \forall k\in\mathcal{K},\ \forall n\in\mathcal{N}. \tag{38}$$

In eq. (38), the values of $\{\hat{\tau}_k\}$ can be expressed as eq. (39), shown at the bottom of the next page, where $\alpha_k=Q^{-1}(\frac{\varepsilon_k^{\max}}{N})$ and $\hat{\beta}_{kn}=\log_2(1+\gamma_{kn}^{\text{off}})$.

*Proof:* Please refer to Appendix E. ∎

### D. Proposed DC Based Algorithm for Solving Problem (OEM-TOP)

After obtaining the optimal solution of $\tau^*$ for Problem (OEM-MID), we introduce a variable $\theta$ as

$$\theta=\sqrt{\tau^*}=\sqrt{\max_{k\in\mathcal{K}}\{\hat{\tau}_k\}}, \tag{40}$$

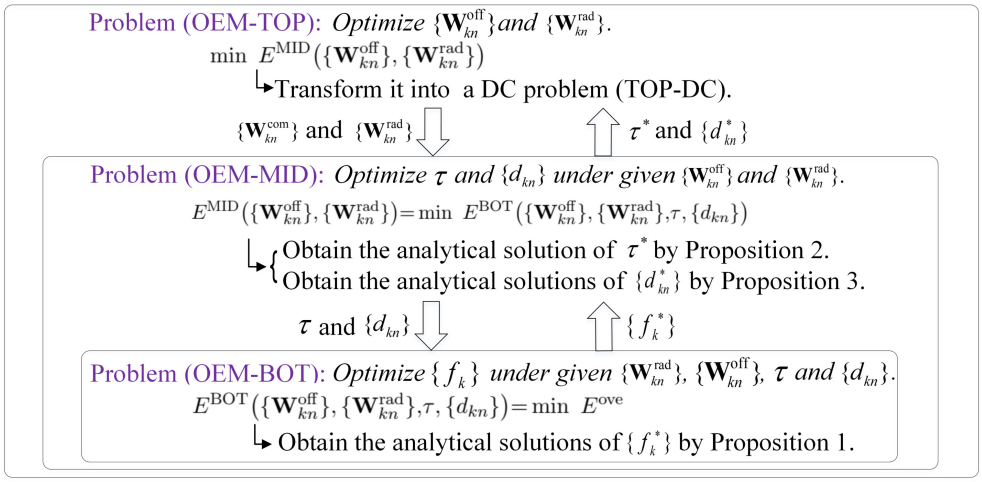


Fig. 2. Hierarchical structure to solve Problem (OEM).

and further substitute $\theta^2$ into Problem (OEM-TOP). As illustrated later in eq. (54), using $\theta^2$ can generate the convex item $(\theta\sqrt{B}\alpha_k+\sum_{n\in\mathcal{N}} z_{kn})^2$ which helps us transform Problem (OEM-TOP) into a DC problem.

By substituting eq. (17), eq. (18), eq. (33) and eq. (40) into the objective function of Problem (OEM-TOP) (i.e., eq. (32)), we can rewrite the objective function of Problem (OEM-TOP) as

$$\varpi_1\theta^2\sum_{n\in\mathcal{N}}\sum_{k\in\mathcal{K}}\text{Tr}(\mathbf{R}_{kn}^{\text{rad}}+\mathbf{R}_{kn}^{\text{off}})+\frac{\sum_{k\in\mathcal{K}}\varpi_2\kappa\zeta^3 D_k^3}{(T^{\max}-N\theta^2)^2}. \tag{41}$$

Recall that constraint (35) comes from constraint (29), and it guarantees the feasibility of Problem (OEM-MID). By substituting eq. (40) into constraint (35), we can rewrite constraint (35) as

$$\theta^2\le\frac{T^{\max}}{N}-\frac{\zeta}{NF^{\text{total}}}\sum_{k\in\mathcal{K}}D_k. \tag{42}$$

In eq. (40), $\gamma_{kn}^{\text{off}}$ is contained in the expression of $\hat{\tau}_k$. The expression of $\gamma_{kn}^{\text{off}}$ contains several items which are norm functions $\|\cdot\|^2$. We next transform it into an equivalent form which contains the items of trace function $\text{Tr}(\cdot)$, since the trace function is linear and easy to address. By denoting $\tilde{\mathbf{H}}_{kn}=\mathbf{h}_{kn}(\mathbf{h}_{kn})^H$, we can transform eq. (13) into

$$\gamma_{kn}^{\text{off}}=\frac{\text{Tr}(\mathbf{R}_{kn}^{\text{off}}\tilde{\mathbf{H}}_{kn})}{\sum_{k\in\mathcal{K}}\text{Tr}(\mathbf{R}_{kn}^{\text{rad}}\tilde{\mathbf{H}}_{kn})+\sum_{j\ne k,j\in\mathcal{K}}\text{Tr}(\mathbf{R}_{jn}^{\text{off}}\tilde{\mathbf{H}}_{jn})+\sigma^2}. \tag{43}$$

By substituting eq. (17) and eq. (18) into constraint (26), we can rewrite constraint (26) into

$$\text{Tr}(\mathbf{R}_{kn}^{\text{rad}}+\mathbf{R}_{kn}^{\text{off}})\le P_k^{\max},\ \forall k\in\mathcal{K},\ \forall n\in\mathcal{N}. \tag{44}$$

Based on the above operations, we can equivalently transform Problem (OEM-TOP) into Problem (TOP-E) as follows, in which constraint (46) and constraint (47) come from eq. (16).

$$\begin{aligned}
\text{(TOP-E):}\quad &\min\ \varpi_1\theta^2\sum_{n\in\mathcal{N}}\sum_{k\in\mathcal{K}}\text{Tr}(\mathbf{R}_{kn}^{\text{rad}}+\mathbf{R}_{kn}^{\text{off}})\\
&\qquad+\frac{\sum_{k\in\mathcal{K}}\varpi_2\kappa\zeta^3 D_k^3}{(T^{\max}-N\theta^2)^2}\\
\text{subject to:}\quad &\theta^2\ge\hat{\tau}_k,\forall k\in\mathcal{K}, &(45)\\
&\mathbf{R}_{kn}^{\text{x}}\succeq 0,\forall k\in\mathcal{K},\forall n\in\mathcal{N}, &(46)\\
&\mathbf{R}_{kn}^{\text{x}}=(\mathbf{R}_{kn}^{\text{x}})^H,\ \forall k\in\mathcal{K},\forall n\in\mathcal{N}, &(47)\\
&\text{constraints: (28), (42), (43), (44),}\\
\text{variables:}\quad &\{\mathbf{R}_{kn}^{\text{off}}\},\{\mathbf{R}_{kn}^{\text{rad}}\},\theta,\{\gamma_{kn}^{\text{off}}\}.
\end{aligned}$$

However, Problem (TOP-E) is still a non-convex optimization problem. We next transform Problem (TOP-E) into a DC problem. We firstly equivalently transform constraint (45) into two constraints (i.e., (49) and (50)), both of which can be transformed into the DC forms. Moreover, we illustrate that other non-convex constraints and the objective function in Problem (TOP-E) can all be transformed into the corresponding DC forms. The detailed procedure is as follows.

*1) Equivalently transforming constraint (45) into two constraints (i.e., (49) and (50))*

In constraint (45), the expression of $\hat{\tau}_k$ is given by eq. (39), which is a complicated function of $\gamma_{kn}^{\text{off}}$. Meanwhile, the expression of $\gamma_{kn}^{\text{off}}$ is given by eq. (13), which is a very complicated function of $\{\mathbf{W}_{kn}^{\text{off}}\}$ and $\{\mathbf{W}_{kn}^{\text{rad}}\}$. If we substitute eq. (13) (i.e., the expression of $\gamma_{kn}^{\text{off}}$) into eq. (39) (i.e., the expression of $\hat{\tau}_k$) and further substitute eq. (39) into constraint (45), we will obtain a very complicated expression which is extremely difficult to deal with. To address this difficulty, we aim at transforming constraint (45) into two constraints, which can

$$\hat{\tau}_k=\left(\frac{\sqrt{B}\alpha_k\sum_{n\in\mathcal{N}}\sqrt{V_{kn}}+\sqrt{B\alpha_k^2\left(\sum_{n\in\mathcal{N}}\sqrt{V_{kn}}\right)^2+4BD_k\sum_{n\in\mathcal{N}}\hat{\beta}_{kn}}}{2B\sum_{n\in\mathcal{N}}\hat{\beta}_{kn}}\right)^2,\forall k\in\mathcal{K}, \tag{39}$$

further be transformed into the DC forms as illustrated later.

In constraint (45) (i.e., $\theta^2 \geq \hat{\tau}_k, \forall k \in \mathcal{K}$), $\hat{\tau}_k$ is the function of $\gamma_{kn}^{\text{off}}$, which is given by eq. (39). We use $\hat{\tau}_k = \hat{f}(\{\gamma_{kn}^{\text{off}}\})$ to denote the function of $\gamma_{kn}^{\text{off}}$ given by eq. (39). Then, we introduce a series of variables $\{z_{kn}\}$ satisfying

$$\theta^2 \geq \hat{f}(\{\frac{1}{\sqrt{1-z_{kn}^2}}-1\}) \geq \hat{f}(\{\gamma_{kn}^{\text{off}}\}), \forall k \in \mathcal{K}. \tag{48}$$

*Remark:* Although we can introduce a series of variables $\{x_{kn}\}$ satisfying $\theta^2 \geq \hat{f}(\{x_{kn}\}) \geq \hat{f}(\{\gamma_{kn}^{\text{off}}\})=\hat{\tau}_k$ to transform constraint (45) into two constraints, it is still difficult for the subsequent transformations. Thus, we introduce variables $\{z_{kn}\}$ satisfying eq. (48), which can transform the expression of $V_{kn}$ in eq. (39) into a simple form.

*Lemma 3:* The function $\hat{f}(\{\gamma_{kn}^{\text{off}}\})$ is monotonically increasing with respect to $\gamma_{kn}^{\text{off}}$.

*Proof:* Please refer to Appendix F. ∎

With Lemma 3 and constraint (48), we can equivalently transform constraint (45) into two constraints as

$$\theta^2 \geq \hat{f}\big(\{\frac{1}{\sqrt{1-z_{kn}^2}}-1\}\big), \quad \forall k \in \mathcal{K}. \tag{49}$$

$$\frac{1}{\sqrt{1-z_{kn}^2}}-1 \geq \gamma_{kn}^{\text{off}}, \quad \forall k \in \mathcal{K}, \forall n \in \mathcal{N}. \tag{50}$$

Eq. (49) is the first part of constraint (48) (i.e., $\theta^2 \geq \hat{f}(\{\frac{1}{\sqrt{1-z_{kn}^2}}-1\})$), and eq. (50) stems from the transformation of the second part of constraint (48) (i.e., $\hat{f}(\{\frac{1}{\sqrt{1-z_{kn}^2}}-1\}) \geq \hat{f}(\{\gamma_{kn}^{\text{off}}\})$) based on the monotonic property in Lemma 3. We next transform constraint (49) and constraint (50) into their respective DC forms.

*2) Transforming constraint (49) into a DC form*

In constraint (49), the expression of function $\hat{f}$ is given by eq. (39). By substituting the expression of $V_{kn}$ (i.e., eq. (4)) into eq. (39), and then substituting eq. (39) into constraint (49), we can rewrite constraint (49) as

$$\sqrt{B\alpha_k^2(\sum_{n\in\mathcal{N}} z_{kn})^2+2BD_k\sum_{n\in\mathcal{N}}\log_2\frac{1}{1-z_{kn}^2}} \leq \theta B\sum_{n\in\mathcal{N}}\log_2\frac{1}{1-z_{kn}^2}-\sqrt{B}\alpha_k\sum_{n\in\mathcal{N}} z_{kn}. \tag{51}$$

By taking square operations on both the left and the right sides of eq. (51) and performing some mathematical manipulations, we can equivalently transform eq. (51) into

$$-\theta^2 B\sum_{n\in\mathcal{N}}\log_2\frac{1}{1-z_{kn}^2}+2\theta\sqrt{B}\alpha_k\sum_{n\in\mathcal{N}} z_{kn}+2D_k \leq 0. \tag{52}$$

In constraint (52), both item $-\theta^2 B\sum_{n\in\mathcal{N}}\log_2\frac{1}{1-z_{kn}^2}$ and item $2\theta\sqrt{B}\alpha_k\sum_{n\in\mathcal{N}} z_{kn}$ are non-convex. We next transform them into the DC forms as follows. By utilizing the property that $xy=\frac{1}{2}(x+y)^2-\frac{1}{2}(x^2+y^2)$, item $-\theta^2 B\sum_{n\in\mathcal{N}}\log_2\frac{1}{1-z_{kn}^2}$ can be equivalently transformed into a DC form as follows (the detailed proof that the right side of eq. (53) is DC can be referred to Appendix G).

$$-\theta^2 B\sum_{n\in\mathcal{N}}\log_2\frac{1}{1-z_{kn}^2} = \frac{B}{2}\Big(\theta^4+\big(\sum_{n\in\mathcal{N}}\log_2\frac{1}{1-z_{kn}^2}\big)^2\Big) - \frac{B}{2}\Big(\theta^2+\sum_{n\in\mathcal{N}}\log_2\frac{1}{1-z_{kn}^2}\Big)^2. \tag{53}$$

Item $2\theta\sqrt{B}\alpha_k\sum_{n\in\mathcal{N}} z_{kn}$ can be transformed into a DC form as follows:

$$2\theta\sqrt{B}\alpha_k\sum_{n\in\mathcal{N}} z_{kn} = \sqrt{B}(\theta^2\alpha_k+\sum_{n\in\mathcal{N}} z_{kn})^2 - \theta^2\sqrt{B}\alpha_k^2-\sqrt{B}(\sum_{n\in\mathcal{N}} z_{kn})^2. \tag{54}$$

By substituting eq. (53) and eq. (54) into constraint (52), we can equivalently transform constraint (52) into the corresponding DC form as

$$-\frac{B}{2}\Big(\theta^2+\sum_{n\in\mathcal{N}}\log_2\frac{1}{1-z_{kn}^2}\Big)^2-\theta^2\sqrt{B}\alpha_k^2-\sqrt{B}(\sum_{n\in\mathcal{N}} z_{kn})^2 +\frac{B}{2}\Big(\theta^4+\big(\sum_{n\in\mathcal{N}}\log_2\frac{1}{1-z_{kn}^2}\big)^2\Big)+\sqrt{B}\Big(\theta\alpha_k+\sum_{n\in\mathcal{N}} z_{kn}\Big)^2 +2D_k \leq 0, \forall k \in \mathcal{K}. \tag{55}$$

*3) Transforming constraint (50) into a DC form*

We next transform constraint (50) into a DC form. By rewriting eq. (50) as $\gamma_{kn}^{\text{off}}+1 \geq \frac{1}{\sqrt{1-z_{kn}^2}}$, $\forall k \in \mathcal{K}, \forall n \in \mathcal{N}$, and then substituting the expression of $\gamma_{kn}^{\text{off}}$ (i.e., eq. (43)) into it, we obtain

$$\frac{1}{\sqrt{1-z_{kn}^2}}\Big(\sum_{k\in\mathcal{K}}\text{Tr}(\mathbf{R}_{kn}^{\text{rad}}\tilde{\mathbf{H}}_{kn})+\sum_{j\neq k,j\in\mathcal{K}}\text{Tr}(\mathbf{R}_{jn}^{\text{off}}\tilde{\mathbf{H}}_{jn})\Big) + \Big(\frac{1}{\sqrt{1-z_{kn}^2}}-1\Big)\sigma^2-\sum_{k\in\mathcal{K}}\text{Tr}(\mathbf{R}_{kn}^{\text{rad}}\tilde{\mathbf{H}}_{kn}) - \sum_{k\in\mathcal{K}}\text{Tr}(\mathbf{R}_{kn}^{\text{off}}\tilde{\mathbf{H}}_{kn}) \leq 0, \forall k \in \mathcal{K}, \forall n \in \mathcal{N}. \tag{56}$$

In eq. (56), all items are convex except item $\frac{1}{\sqrt{1-z_{kn}^2}}(\sum_{k\in\mathcal{K}}\text{Tr}(\mathbf{R}_{kn}^{\text{rad}}\tilde{\mathbf{H}}_{kn})+\sum_{j\neq k,j\in\mathcal{K}}\text{Tr}(\mathbf{R}_{jn}^{\text{off}}\tilde{\mathbf{H}}_{jn}))$, which is the product of i) a convex item $\frac{1}{\sqrt{1-z_{kn}^2}}$ and ii) a linear item $(\sum_{k\in\mathcal{K}}\text{Tr}(\mathbf{R}_{kn}^{\text{rad}}\tilde{\mathbf{H}}_{kn})+\sum_{j\neq k,j\in\mathcal{K}}\text{Tr}(\mathbf{R}_{jn}^{\text{off}}\tilde{\mathbf{H}}_{jn}))$. In particular, item $\frac{1}{\sqrt{1-z_{kn}^2}}(\sum_{k\in\mathcal{K}}\text{Tr}(\mathbf{R}_{kn}^{\text{rad}}\tilde{\mathbf{H}}_{kn})+\sum_{j\neq k,j\in\mathcal{K}}\text{Tr}(\mathbf{R}_{jn}^{\text{off}}\tilde{\mathbf{H}}_{jn}))$ can be transformed into a DC form as follows (the detailed proof that the right side of eq. (57) is DC can be referred to Appendix H).

$$\frac{1}{\sqrt{1-z_{kn}^2}}\Big(\sum_{k\in\mathcal{K}}\text{Tr}(\mathbf{R}_{kn}^{\text{rad}}\tilde{\mathbf{H}}_{kn})+\sum_{j\neq k,j\in\mathcal{K}}\text{Tr}(\mathbf{R}_{jn}^{\text{off}}\tilde{\mathbf{H}}_{jn})\Big) = \frac{1}{2}\Big(\frac{1}{\sqrt{1-z_{kn}^2}}+\sum_{k\in\mathcal{K}}\text{Tr}(\mathbf{R}_{kn}^{\text{rad}}\tilde{\mathbf{H}}_{kn})+\sum_{j\neq k,j\in\mathcal{K}} \text{Tr}(\mathbf{R}_{jn}^{\text{off}}\tilde{\mathbf{H}}_{jn})\Big)^2-\frac{1}{2}\Big(\frac{1}{1-z_{kn}^2} +\Big(\sum_{k\in\mathcal{K}}\text{Tr}(\mathbf{R}_{kn}^{\text{rad}}\tilde{\mathbf{H}}_{kn})+\sum_{j\neq k,j\in\mathcal{K}}\text{Tr}(\mathbf{R}_{jn}^{\text{off}}\tilde{\mathbf{H}}_{jn})\Big)^2\Big). \tag{57}$$

By substituting eq. (57) into constraint (56), we can transform constraint (56) into a DC form as follows:

$$\begin{aligned}&\frac{1}{2}\Big(\frac{1}{\sqrt{1-z_{kn}^2}}+\sum_{k\in\mathcal{K}}\mathrm{Tr}(\mathbf{R}_{kn}^{\mathrm{rad}}\tilde{\mathbf{H}}_{kn})+\sum_{j\neq k,j\in\mathcal{K}}\mathrm{Tr}(\mathbf{R}_{jn}^{\mathrm{off}}\tilde{\mathbf{H}}_{jn})\Big)^2\\&-\frac{1}{2}\Big(\frac{1}{1-z_{kn}^2}+\Big(\sum_{k\in\mathcal{K}}\mathrm{Tr}(\mathbf{R}_{kn}^{\mathrm{rad}}\tilde{\mathbf{H}}_{kn})\\&+\sum_{j\neq k,j\in\mathcal{K}}\mathrm{Tr}(\mathbf{R}_{jn}^{\mathrm{off}}\tilde{\mathbf{H}}_{jn})\Big)^2\Big)+(\frac{1}{\sqrt{1-z_{kn}^2}}-1)\sigma^2\\&-\sum_{k\in\mathcal{K}}\mathrm{Tr}(\mathbf{R}_{kn}^{\mathrm{rad}}\tilde{\mathbf{H}}_{kn})-\sum_{k\in\mathcal{K}}\mathrm{Tr}(\mathbf{R}_{kn}^{\mathrm{off}}\tilde{\mathbf{H}}_{kn})\\&\leq 0,\quad \forall k\in\mathcal{K},\,\forall n\in\mathcal{N}.\end{aligned}\tag{58}$$

*4) Transforming constraint (28) into a DC form*

We next transform constraint (28) (i.e., $I_{kn}^{\mathrm{rad}}\geq I_{kn}^{\min}$) into a DC form. By utilizing the property that $\det(\mathbf{X}^{-1}\mathbf{Y})=\frac{\det(\mathbf{Y})}{\det(\mathbf{X})}$, we can rewrite $I_{kn}^{\mathrm{rad}}$ as

$$I_{kn}^{\mathrm{rad}}=B\log\det(\mathbf{\Phi}_{kn}+\mathbf{A}_{kn}\mathbf{R}_{kn}^{\mathrm{rad}}\mathbf{A}_{kn}^H)-B\log\det(\mathbf{\Phi}_{kn}).\tag{59}$$

By substituting eq. (59) into constraint (28), we can transform constraint (28) into a DC form as follows:

$$\begin{aligned}&-B\log\det(\mathbf{\Phi}_{kn}+\mathbf{A}_{kn}\mathbf{R}_{kn}^{\mathrm{rad}}\mathbf{A}_{kn}^H)+B\log\det(\mathbf{\Phi}_{kn})+I_{kn}^{\min}\\&\leq 0,\quad \forall k\in\mathcal{K},\,\forall n\in\mathcal{N},\end{aligned}\tag{60}$$

where the expression of $\mathbf{\Phi}_{kn}$ is given by eq. (20) before. The reason for concluding that the left side of (60) is the difference of convexity is that the logarithm-determinant function $\log\det(\cdot)$ is concave [37].

*5) Transforming Problem (TOP-E) into a DC problem*

In the objective function of Problem (TOP-E), $\frac{\sum_{k\in\mathcal{K}}\varpi_2\kappa\zeta^3D_k^3}{(T^{\max}-N\theta^2)^2}$ is convex according to the operation rules of preserving convexity for composition function. However, $\varpi_1\theta^2\sum_{n\in\mathcal{N}}\sum_{k\in\mathcal{K}}\mathrm{Tr}(\mathbf{R}_{kn}^{\mathrm{rad}}+\mathbf{R}_{kn}^{\mathrm{off}})$ is non-convex, which is the product of i) a convex function $\varpi_1\theta^2$ and ii) a linear function $\sum_{n\in\mathcal{N}}\mathrm{Tr}(\mathbf{R}_{kn}^{\mathrm{rad}}+\mathbf{R}_{kn}^{\mathrm{off}})$. By again utilizing the property that $xy=\frac{1}{2}(x+y)^2-\frac{1}{2}(x^2+y^2)$, we can further transform $\varpi_1\theta^2\sum_{n\in\mathcal{N}}\sum_{k\in\mathcal{K}}\mathrm{Tr}(\mathbf{R}_{kn}^{\mathrm{rad}}+\mathbf{R}_{kn}^{\mathrm{off}})$ into a DC form as follows:

$$\begin{aligned}&\varpi_1\theta^2\sum_{n\in\mathcal{N}}\sum_{k\in\mathcal{K}}\mathrm{Tr}(\mathbf{R}_{kn}^{\mathrm{rad}}+\mathbf{R}_{kn}^{\mathrm{off}})\\&=\frac{1}{2}\Big(\varpi_1\theta^2+\sum_{n\in\mathcal{N}}\sum_{k\in\mathcal{K}}\mathrm{Tr}(\mathbf{R}_{kn}^{\mathrm{rad}}+\mathbf{R}_{kn}^{\mathrm{off}})\Big)^2-\frac{1}{2}(\varpi_1\theta^2)^2\\&-\frac{1}{2}\Big(\sum_{n\in\mathcal{N}}\sum_{k\in\mathcal{K}}\mathrm{Tr}(\mathbf{R}_{kn}^{\mathrm{rad}}+\mathbf{R}_{kn}^{\mathrm{off}})\Big)^2.\end{aligned}\tag{61}$$

By substituting eq. (61) into the objective function of Problem (TOP-E), and also considering the previous transformations in eqs. (55), (58) and (60), we can equivalently transform Problem (TOP-E) into a DC problem (TOP-DC) as follows.

$$\begin{aligned}\text{(TOP-DC):}\ \min\ &\frac{1}{2}\Big(\varpi_1\theta^2+\sum_{n\in\mathcal{N}}\sum_{k\in\mathcal{K}}\mathrm{Tr}(\mathbf{R}_{kn}^{\mathrm{rad}}+\mathbf{R}_{kn}^{\mathrm{off}})\Big)^2\\&-\frac{1}{2}\Big(\sum_{n\in\mathcal{N}}\sum_{k\in\mathcal{K}}\mathrm{Tr}(\mathbf{R}_{kn}^{\mathrm{rad}}+\mathbf{R}_{kn}^{\mathrm{off}})\Big)^2\\&+\frac{\sum_{k\in\mathcal{K}}\varpi_2\kappa\zeta^3D_k^3}{(T^{\max}-N\theta^2)^2}-\frac{1}{2}(\varpi_1\theta^2)^2\\\text{subject to:}\ &\text{constraints: (42), (44), (46), (47), (55), (58), (60),}\\&\text{variables: }\{\mathbf{R}_{kn}^{\mathrm{off}}\},\{\mathbf{R}_{kn}^{\mathrm{rad}}\},\theta,\{z_{kn}\}.\end{aligned}$$

**Algorithm 1** Proposed Algorithm to Solve Problem (OEM)

1: Compute the optimal solutions of $\{\mathbf{W}_{kn}^{\mathrm{off}}\}$ and $\{\mathbf{W}_{kn}^{\mathrm{rad}}\}$ by solving Problem (TOP-DC) with the DC algorithm.
2: Compute the optimal solutions of $\{d_{kn}\}$ according to eq. (38) in Proposition 3.
3: Compute the optimal solution of $\tau$ according to eq. (36) in Proposition 2.
4: Compute the optimal solutions of $\{f_k\}$ according to eq. (31) in Proposition 1.
5: **output:** the optimal solutions of $\{\mathbf{W}_{kn}^{\mathrm{off}}\}$ and $\{\mathbf{W}_{kn}^{\mathrm{rad}}\}$, $\{d_{kn}\}$, $\tau$ and $\{f_k\}$.

As a DC optimization problem, Problem (TOP-DC) can be solved by several existing methods, e.g., the DC algorithm [38]. After obtaining the optimal solutions of $\{\mathbf{R}_{kn}^{\mathrm{off}}\}$ and $\{\mathbf{R}_{kn}^{\mathrm{rad}}\}$, we can utilize the singular value decomposition [39] to recover the optimal solutions of $\{\mathbf{W}_{kn}^{\mathrm{off}}\}$ and $\{\mathbf{W}_{kn}^{\mathrm{rad}}\}$.

### *E. Proposed Overall Algorithm for Solving Problem (OEM)*

As a summary of the optimal solutions of our top-layer, middle-layer, and bottom-layer problems, we present the overall algorithm for solving Problem (OEM) as Algorithm 1 below. A key advantage is that our Algorithm 1 does not require any alternative iteration among the bottom-layer, middle-layer, and top-layer problems. Specifically, we can use the DC algorithm to solve Problem (OEM-TOP), which provides the optimal solutions for the beamformings for radar sensing and offloading transmission. With the above optimal beamformings, we can compute the remaining parts of the optimal solutions of Problem (OEM) by using the analytical solutions characterized in Propositions 1, 2, and 3. The DC algorithm is used in Step 1. In spite of its guaranteed convergence, the DC algorithm may converge to a local optimal solution for Problem (TOP-DC). Nevertheless, it is technically challenging to provide a quantitative analysis on the potential gap between the solution of the DC algorithm and the globally optimal one, which is still an open question even in the areas of optimization research.

Since Propositions 1, 2, and 3 provide the analytical solutions for the respective variables, the complexity of Algorithm 1 is dominated by solving Problem (TOP-DC) via the DC algorithm and the subsequent singular value decomposition. The DC algorithm requires to iteratively solve a semi-definite program problem, whose computing complexity is $\mathcal{O}(M^2KN)$ by utilizing the path-following method in [40] (Recall that $M$ denotes the number of antennas on the ISAC devices). The computing complexity for the singular value decomposition is $\mathcal{O}(M^3)$ [22]. Thus, the overall computing

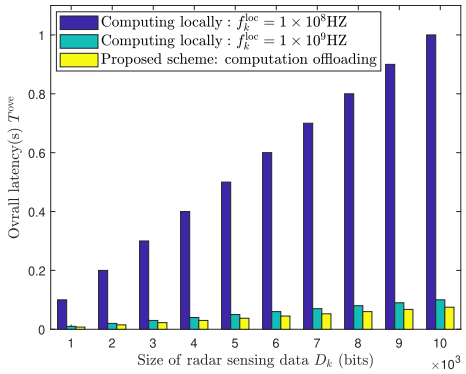


Fig. 3. Comparison with the non-offloading scheme.

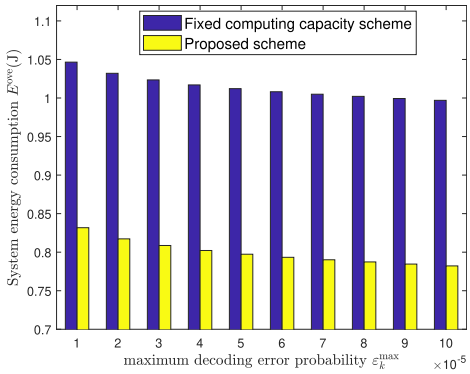


Fig. 4. Comparison with the scheme of fixed edge-server's computing capacity allocation.

complexity of our proposed algorithm solving Problem (OEM) is $\mathcal{O}(M^2KN + M^3)$.

## V. Numerical Results

We show the numerical results to validate the performances of our MEC aided ISAC with short-packet transmissions and our proposed algorithm. The AP, which is co-located with the edge-server, is located at $(0\text{m}, 0\text{m})$. The ISAC devices are randomly located in a circular region, and its center is located at the AP and its radius is 50m. The channel gain is modeled as $\mathbf{h}_k = \sqrt{\text{PL}_k}\mathbf{g}_k$. $\text{PL}_k$ is the large scale path loss which is modeled with the unit dB as $\text{PL}_k = \text{PL}_0 - 10\alpha \log_{10}\frac{L_k}{L_0}$, where $\text{PL}_0$ represents the path loss at the reference distance $L_0$, $L_k$ is the distance between the ISAC device $k$ and the AP, and $\alpha$ is the path loss exponent. $\mathbf{g}_k$ is the small scale fading whose value follows the zero mean complex Gaussian distribution. Similar to [15] and [22], we set the parameters as follows. $D_k \in [1,2] \times 10^3$ bits, $F^{\text{total}} = 2 \times 10^{10}$ HZ, $\kappa = 1 \times 10^{-26}$, $B = 5 \times 10^6$ HZ, $\sigma^2 = 1 \times 10^{-14}$, $\text{PL}_0 = 30$ dB, $L_0 = 1$ m, $\alpha = 2$, $\varepsilon_k^{\max} \in [1,2] \times 10^{-5}$, $T^{\max} = 0.2$ s, $\zeta = 1 \times 10^3$ cycles/bit.

### A. Evaluation of the Proposed Scheme

Figure 3 shows the performance of the proposed scheme in comparison with the non-offloading scheme where the radar-sensing data is analyzed locally on the ISAC devices. In Figure 3, $f_k^{\text{loc}}$ denotes the computing-capacity of ISAC device $k$, and we set the same value of $f_k^{\text{loc}}$ for all ISAC devices. We set the same value of $D_k$ for all ISAC devices. It can be seen that our proposed MEC aided ISAC scheme can achieve a lower latency compared with the non-offloading scheme. Our scheme can leverage the sufficient computing resources at the edge-server to reduce the latency for sensing data analysis.

Figure 4 shows the performance of the proposed scheme in comparison with the scheme of fixed edge-server's computing capacity allocation. It can be seen that the proposed scheme can achieve lower energy consumption due to the optimized edge-server's computing capacity allocation. In addition, the system energy consumption is decreasing with respect to the maximum decoding error probability. The reason is that increasing the maximum decoding error probability can increase the feasible region restrained by constraint (9) (i.e., the decoding error probability constraint).

Figure 5 shows the performance of the proposed scheme in comparison with the equal packet size allocation (EQPS) scheme. Specifically, in EQPS scheme, we set $d_{k1} = d_{k2} = \ldots = d_{kN}$, $\forall k \in \mathcal{K}$. We set the same value of $D_k$ for all ISAC devices. It can be seen from Figure 5 that our proposed scheme with the optimized packet sizes can achieve a better performance than the EQPS scheme. To adapt to the time-varying channel, using different packet sizes in different time-slots can yield a smaller energy consumption than using a fixed packet size. It can also be observed from Figure 5 that the energy consumption is increasing with the data size of the radar-sensing data, which is consistent with our intuition.

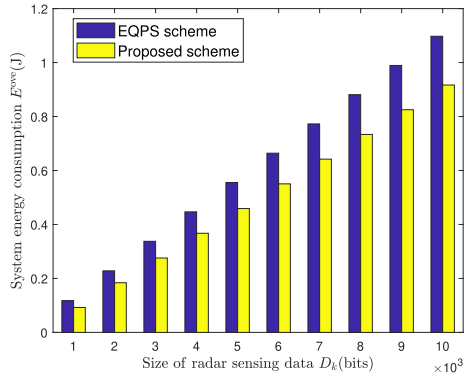


Fig. 5. Comparison with the EQPS scheme.

Figure 6 shows the performance of the proposed scheme in comparison with the random packet size allocation (RNPS) scheme. Specifically, in RNPS scheme, we randomly allocate the overall datasize into each packet. It can be seen that our proposed scheme can achieve a smaller energy consumption in comparison with the RNPS scheme. It can also be observed from Figure 6 that using a larger value of the maximum decoding error probability can reduce the energy consumption.

Figure 7 and Figure 8 show the performance of the proposed scheme in comparison with the FixedDuration scheme under $K = 3$ and $K = 5$, respectively. Here, FixedDuration represents "fixed duration of each short packet". Figure 7 and Figure 8 show the benefit of optimizing the duration of each short packet in our proposed scheme. Optimizing the duration of each short packet enables the ISAC devices to efficiently adjust their transmit-power and the offloading latency to achieve a smaller energy consumption. Moreover, it can be seen from Figure 7 and Figure 8 that the energy consumption is increasing with the number of ISAC devices.

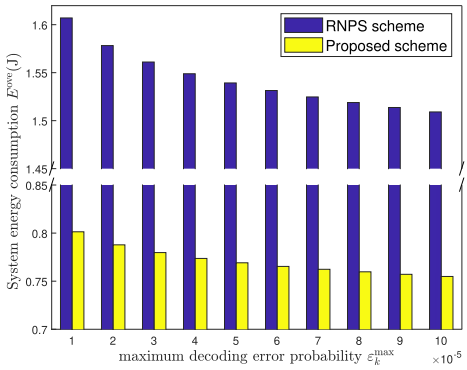


Fig. 6. Comparison with the RNPS scheme.

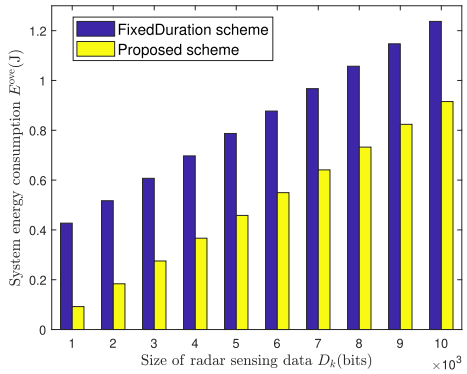


Fig. 7. Comparison with the fixed short packet duration scheme: $K = 3$.

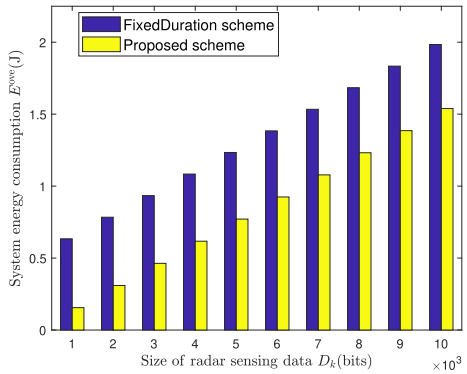


Fig. 8. Comparison with the fixed short packet duration scheme: $K = 5$.

### B. Evaluation of Our Proposed Algorithm

We evaluate the performance of the proposed algorithm by comparing it with two benchmarks as follows.

- BCD-SO-AS algorithm. We utilize the block coordinate descent (BCD) method to divide Problem (OEM) into three subproblems as follows. i) The first subproblem is to optimize $\{f_k\}_{\mathcal{K}}$, which is solved by the active-set (AS) algorithm [41]. ii) The second subproblem is to optimize $\{d_{kn}\}$ and $\tau$, which is solved by the AS algorithm as well. iii) The third subproblem is to optimize $\{\mathbf{W}_{kn}^{\text{rad}}\}$ and $\{\mathbf{W}_{kn}^{\text{off}}\}$, which is solved by the surrogate optimization (SO) algorithm [42].
- BCD-PS-SQP algorithm. We utilize the BCD method to divide Problem (OEM) into three subproblems as follows. i) The first subproblem is to optimize $\{f_k\}_{\mathcal{K}}$, which is solved by the sequential quadratic programing (SQP) algorithm [43]. ii) The second subproblem is to optimize $\{d_{kn}\}$ and $\tau$, which is solved by the SQP algorithm as well. iii) The third subproblem is to optimize $\{\mathbf{W}_{kn}^{\text{rad}}\}$ and $\{\mathbf{W}_{kn}^{\text{off}}\}$, which is solved by the pattern search (PS) optimization algorithm [44].

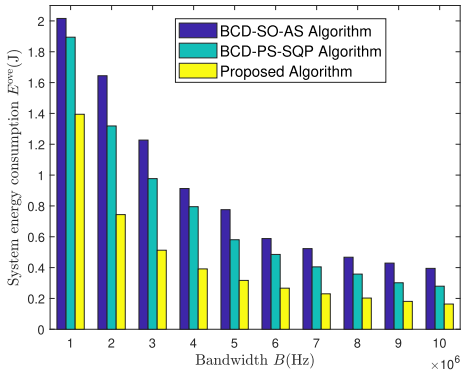


Fig. 9. Comparison under different values of the channel bandwidth.

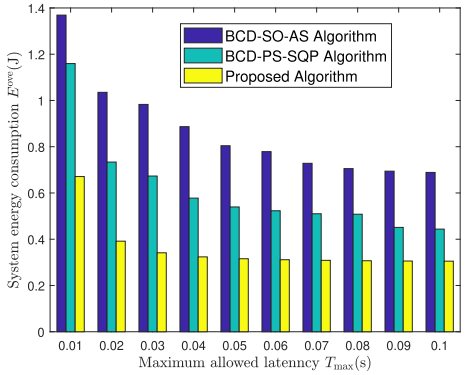


Fig. 10. Comparison under different values of the maximum allowed latency.

Figure 9 shows the comparison between our proposed algorithm and two benchmark schemes versus different channel bandwidths. It can be seen that the system energy consumption is decreasing with respect to the bandwidth. Figure 9 shows that our proposed algorithm can outperform both BCD-SO-AS algorithm and BCD-PS-SQP algorithm. We identify the special features of our formulated problem (e.g., Proposition 1, Proposition 2 and Proposition 3) to compute the optimal solutions efficiently, which thus yields a better performance than the benchmark algorithms.

Figure 10 shows the comparison between our proposed algorithm and two benchmark schemes versus different maximum latency allowed. It can be seen from Figure 10 that the system energy consumption is decreasing with respect to the maximum allowed latency. Figure 10 shows that our proposed algorithm can outperform both BCD-SO-AS algorithm and BCD-PS-SQP algorithm.

## VI. Conclusion

In this paper, we have proposed a paradigm of MEC aided ISAC with short-packet transmissions, where the ISAC devices reliably offload their radar-sensing data to an edge-server for analysis via short-packet transmissions. An energy minimization problem is formulated, in which we have jointly optimized the beamforming for offloading transmission, the beamforming for radar sensing, the computing-capacity allocations of the edge-server, the duration of each short packet, and the size of each short packet. We have exploited the hierarchical structure of our problem and have proposed an efficient algorithm to

compute the solutions. The simulation results show the advantage of our proposed scheme and our proposed algorithm. In the future work, we will study the scenario of multiple edge-servers providing the task processing services, in which each ISAC device can flexibly select different edge-servers to offload its radar-sensing data for analysis.

## APPENDIX A
## PROOF OF PROPOSITION 1

By substituting eq. (21) into eq. (22), and then substituting eq. (22) into constraint (27), we can equivalently transform constraint (27) into

$$N\tau+\frac{\zeta D_k}{f_k}\leq T^{\max},\forall k\in\mathcal{K}. \tag{62}$$

From eq. (62), we obtain

$$f_k\geq\frac{\zeta D_k}{T^{\max}-N\tau},\forall k\in\mathcal{K}. \tag{63}$$

Constraint (63) gives the lower boundary of the feasible region for $\{f_k\}$. Meanwhile, constraint (29) gives the upper boundary of the feasible region for $\{f_k\}$. To guarantee the feasibility of Problem (OEM-BOT), the upper boundary given by constraint (29) must be larger than the lower boundary given by constraint (63). By substituting the lower boundary given by constraint (63) into eq. (29), we obtain

$$\sum_{k\in\mathcal{K}}\frac{\zeta D_k}{T^{\max}-N\tau}\leq F^{\text{total}}. \tag{64}$$

From eq. (64), we can obtain eq. (30) in Proposition 1.

In the objective function of Problem (OEM-BOT), all items are fixed except item $\varpi_2\sum_{k\in\mathcal{K}}\kappa\zeta D_k f_k^2$. Thus, to minimize the objective of Problem (OEM-BOT) is equivalent to minimize $\sum_{k\in\mathcal{K}}\kappa\zeta D_k f_k^2$. To minimize $\sum_{k\in\mathcal{K}}\kappa\zeta D_k f_k^2$, we should decrease each value of $f_k$ for each device until it reaches its lower boundary of its feasible region. Constraint (63) gives the lower boundary of the feasible region for $f_k$. Thus, the optimal values of $\{f_k\}$ for Problem (OEM-BOT) are given by eq. (31) in Proposition 1.

## APPENDIX B
## PROOF OF LEMMA 1

We introduce a variable as $\bar{x}=\sqrt{B\tau}$, and denote

$$\bar{y}_{kn}=\sqrt{\frac{1}{V_{kn}}}\log_2(1+\gamma_{kn}^{\text{off}})\bar{x}-\frac{d_{kn}}{\sqrt{V_{kn}}\bar{x}}. \tag{65}$$

Then, the expression of $\varepsilon_{kn}$ can be expressed as $\varepsilon_{kn}=Q(\bar{y}_{kn})$.

In particular, the first order derivative of $\bar{y}_{kn}$ can be expressed as

$$\frac{d\,\bar{y}_{kn}}{d\,\bar{x}}=\sqrt{\frac{1}{V_{kn}}}\log_2(1+\gamma_{kn}^{\text{off}})+\frac{d_{kn}}{\sqrt{V_{kn}}\bar{x}^2}>0, \tag{66}$$

which means that $\bar{y}_{kn}$ is monotonically increasing with $\bar{x}$. Since the Q-function is monotonically decreasing [25], [30], $\varepsilon_{kn}$ is monotonically decreasing with $\bar{y}_{kn}$. $\bar{y}_{kn}$ is monotonically increasing with $\bar{x}$ and $\bar{x}$ is monotonically increasing with $\tau$. Thus, we can conclude that $\varepsilon_{kn}$ is monotonically decreasing with $\tau$. From the expression of $\varepsilon_k$ in eq. (7), we can conclude that $\varepsilon_k$ is monotonically decreasing with $\tau$.

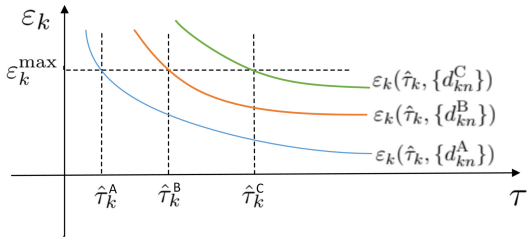


Fig. 11. The value of $\hat{\tau}_k$ under different values of $\{d_{kn}\}_{n\in\mathcal{N}}$.

## APPENDIX C
## PROOF OF PROPOSITION 2

Since $\varepsilon_k$ is monotonically decreasing with $\tau$, constraint (9) (i.e., $\varepsilon_k\leq\varepsilon_k^{\max}$) can be transformed into

$$\tau\geq\hat{\tau}_k,\ \forall k\in\mathcal{K}. \tag{67}$$

Constraint (67) gives the lower boundary of the feasible region for $\tau$. Meanwhile, constraint (30) gives the upper boundary of the feasible region for $\tau$. To guarantee the feasibility of Problem (OEM-MID), the upper boundary given by constraint (30) should be larger than the lower boundary given by constraint (67). By substituting the lower boundary given by constraint (67) into eq. (30), we obtain eq. (35) in Proposition 2.

As illustrated before, the objective function of Problem (OEM-BOT) is transformed into eq. (32). We use $g(\tau)$ to denote the objective function of Problem (OEM-MID), i.e.,

$$g(\tau)=\varpi_1\tau\hat{u}+\frac{\varpi_2\kappa\zeta^3\sum_{k\in\mathcal{K}}D_k^3}{(T^{\max}-N\tau)^2}. \tag{68}$$

The first order of $g(\tau)$ can be expressed as

$$g'(\tau)=\varpi_1\hat{u}+\frac{2N\varpi_2\kappa\zeta^3\sum_{k\in\mathcal{K}}D_k^3}{(T^{\max}-N\tau)^3}>0, \tag{69}$$

which means that $g(\tau)$ is monotonically increasing with $\tau$. Thus, to minimize $g(\tau)$, we need to decrease $\tau$ until it reaches its lower boundary of its feasible region. Eq. (67) gives the lower boundary for $\tau$. Thus, the optimal solution of $\tau$ can be expressed as eq. (36) in Proposition 2.

## APPENDIX D
## PROOF OF LEMMA 2

As shown in the proof of Proposition 2, the objective value of Problem (OEM-MID) is monotonically increasing with $\tau$. To decrease the objective value of Problem (OEM-MID), we should decrease the value of $\tau$. From eq. (36) in Proposition 2, to decrease $\tau$, we should decrease each value of $\hat{\tau}_k$. $\hat{\tau}_k$ is coupled with $\{d_{kn}\}_{n\in\mathcal{N}}$ in eq. (34). We conduct the analysis of $\hat{\tau}_k$ and $\{d_{kn}\}_{n\in\mathcal{N}}$ in eq. (34) as follows.

As shown in Figure 11, different values of $\{d_{kn}\}_{n\in\mathcal{N}}$ generate different curves, which correspond to different functions of $\varepsilon_k$ with respected to $\tau$. $\{\hat{\tau}_k\}_{\mathcal{K}}$ are the cross points of these curves and the line $\varepsilon_k=\varepsilon_k^{\max}$. For instance, $\{d_{kn}^{\text{A}}\}_{n\in\mathcal{N}}$ corresponds to $\hat{\tau}_k^{\text{A}}$, $\{d_{kn}^{\text{B}}\}_{n\in\mathcal{N}}$ corresponds to $\hat{\tau}_k^{\text{B}}$, $\{d_{kn}^{\text{C}}\}_{n\in\mathcal{N}}$ corresponds to $\hat{\tau}_k^{\text{C}}$. As illustrated before, to decrease the objective value of Problem (OEM-MID), we need to decrease the value of $\tau$. To decrease the value of $\hat{\tau}_k$, we should adjust

the values of $\{d_{kn}\}_{n\in\mathcal{N}}$ to move down the curve of $\varepsilon_k$ which represents the function of $\varepsilon_k$ with respected to $\tau$. In other other words, we should adjust the values of $\{d_{kn}\}_{n\in\mathcal{N}}$ to decrease $\varepsilon_k$.

By utilizing the arithmetic-geometric mean inequality, we can conclude that

$$\varepsilon_k=\sum_{n\in\mathcal{N}}\varepsilon_{kn}(\hat{\tau}_k,d_{kn})\geq N\sqrt[N]{\prod_{n\in\mathcal{N}}\varepsilon_{kn}(\hat{\tau}_k,d_{kn})}. \tag{70}$$

In eq. (70), when

$$\varepsilon_{k1}(\hat{\tau}_k,d_{k1})=\varepsilon_{k2}(\hat{\tau}_k,d_{k2})=\ldots=\varepsilon_{kN}(\hat{\tau}_k,d_{kN}), \tag{71}$$

$\varepsilon_k$ achieves its minimum value, and the following equality holds:

$$\varepsilon_k=\sum_{n\in\mathcal{N}}\varepsilon_{kn}(\hat{\tau}_k,d_{kn})=N\sqrt[N]{\prod_{n\in\mathcal{N}}\varepsilon_{kn}(\hat{\tau}_k,d_{kn})}. \tag{72}$$

Since we should decrease $\varepsilon_k$ to move down the curve of $\varepsilon_k$, and $\varepsilon_k$ achieves its minimum value when eq. (71) is satisfied, we can conclude that the optimal solutions of $\{d_{kn}\}$ should satisfy eq. (37) in Lemma 2. On the other hand, Lemma 2 can be also validated by showing the contradiction. Specifically, if the optimal solutions of $\{d_{kn}\}$ do not satisfy eq. (37), we can always adjust the values of $\{d_{kn}\}$ such that an even smaller value of $\hat{\tau}_k$ can be achieved, which leads to an even smaller objective value of Problem (OEM-MID).

## Appendix E
## Proof of Proposition 3

Eq. (37) in Lemma 2 can be rewritten as

$$\varepsilon_{kn}(\hat{\tau}_k,d_{kn})=\frac{\varepsilon_k^{\max}}{N},\forall n\in\mathcal{N},\forall k\in\mathcal{K}. \tag{73}$$

By substituting eq. (6) into eq. (73), we can obtain eq. (38) in Proposition 3. By substituting eq. (38) into eq. (2) (i.e., $\sum_{n\in\mathcal{N}}d_{kn}=D_k$), we obtain

$$B\hat{\tau}_k\sum_{n\in\mathcal{N}}\log_2(1+\gamma_{kn}^{\text{off}})-\sqrt{B\hat{\tau}_k}Q^{-1}(\frac{\varepsilon_k^{\max}}{N})\sum_{n\in\mathcal{N}}\sqrt{V_{kn}}=D_k. \tag{74}$$

We denote

$$\hat{a}_k=B\sum_{n\in\mathcal{N}}\log_2(1+\gamma_{kn}^{\text{off}}), \tag{75}$$

$$\hat{b}_k=\sqrt{B}Q^{-1}(\frac{\varepsilon_k^{\max}}{N})\sum_{n\in\mathcal{N}}\sqrt{V_{kn}}, \tag{76}$$

Then, eq. (74) can be written as

$$\hat{a}_k(\sqrt{\hat{\tau}_k})^2-\hat{b}_k\sqrt{\hat{\tau}_k}-D_k=0. \tag{77}$$

The left side of eq. (77) is the quadratic function of $\sqrt{\hat{\tau}_k}$. By ignoring the negative root (which is infeasible) of eq. (77), we can obtain the solution of $\hat{\tau}_k$ as

$$\hat{\tau}_k=\Big(\frac{\hat{b}_k+\sqrt{\hat{b}_k^2+4\hat{a}_kD_k}}{2\hat{a}_k}\Big)^2. \tag{78}$$

By substituting eq. (75) and eq. (76) into eq. (78), we obtain eq. (39) in Proposition 3.

## Appendix F
## Proof of Lemma 3

By substituting the expression of $V_{kn}$ (i.e., eq. (4)) into $\hat{f}(\{\gamma_{kn}^{\text{off}}\})$ (i.e., eq. (39)), and by denoting $x_{kn}=\frac{1}{(1+\gamma_{kn}^{\text{off}})^2}$, we can transform function $\hat{f}(\{\gamma_{kn}^{\text{off}}\})$ into

$$\hat{f}(x_{kn})=\frac{\sqrt{\alpha_k^2(\sum_{n\in\mathcal{N}}(1-x_{kn}))^2-2(\ln 2)^4D_k\sum_{n\in\mathcal{N}}\log_2 x_{kn}}}{-\sqrt{B}(\ln 2)^2\sum_{n\in\mathcal{N}}\log_2 x_{kn}}+\frac{\alpha_k\sum_{n\in\mathcal{N}}(1-x_{kn})}{-\sqrt{B}(\ln 2)^2\sum_{n\in\mathcal{N}}\log_2 x_{kn}}. \tag{79}$$

The first order derivative of $\hat{f}(x_{kn})$ can be expressed as

$$\frac{\partial\hat{f}}{\partial x_{kn}}=\frac{(\alpha_k+\frac{\alpha_k^2\sum_{n\in\mathcal{N}}(1-x_{kn})+(\ln 2)^3BD_k\frac{1}{x_{kn}}}{\sqrt{\alpha_k^2(\sum_{n\in\mathcal{N}}(1-x_{kn}))^2-2(\ln 2)^4D_k\sum_{n\in\mathcal{N}}\log_2 x_{kn}}})}{\sqrt{B}(\ln 2)^2\sum_{n\in\mathcal{N}}\log_2 x_{kn}}+\frac{\sqrt{\frac{\alpha_k^2}{(\ln 2)^4}(\sum_{n\in\mathcal{N}}(1-x_{kn}))^2-2D_k\sum_{n\in\mathcal{N}}\log_2 x_{kn}}}{x_{kn}\sqrt{B}(\ln 2)(\sum_{n\in\mathcal{N}}\log_2 x_{kn})^2}+\frac{\alpha_k\sum_{n\in\mathcal{N}}(1-x_{kn})}{x_{kn}\sqrt{B}(\ln 2)^3(\sum_{n\in\mathcal{N}}\log_2 x_{kn})^2} \tag{80}$$

Since $0<x_{kn}<1$, from the above equation, we can conclude that

$$\frac{\partial\hat{f}}{\partial x_{kn}}>0,\ \forall k\in\mathcal{K},\ \forall n\in\mathcal{N}. \tag{81}$$

From eq. (81), we can obtain the result in Lemma 3.

## Appendix G
## Proof of the DC Property of Eq. (53)

Since $\sum_{n\in\mathcal{N}}\log_2\frac{1}{(1-z_{kn}^2)}=-\sum_{n\in\mathcal{N}}\log_2(1-z_{kn}^2)$, according to the operation rules of preserving convexity for composition function [37], we can conclude that $\sum_{n\in\mathcal{N}}\log_2\frac{1}{(1-z_{kn}^2)}$ is convex. Also according to the operation rules of preserving convexity for composition function, we can conclude that both item $\big(\theta^2+\sum_{n\in\mathcal{N}}\log_2\frac{1}{(1-z_{kn}^2)}\big)^2$ and item $\big(\sum_{n\in\mathcal{N}}\log_2\frac{1}{(1-z_{kn}^2)}\big)^2$ are convex. Thus, the right side of eq. (53) is DC.

## Appendix H
## Proof of the DC Property of Eq. (57)

According to the operation rules of preserving convexity for composition function, we can conclude that $\frac{1}{\sqrt{1-z_{kn}^2}}$ and $\frac{1}{1-z_{kn}^2}$ are convex. Also according to the operation rules of preserving convexity for composition function, we can conclude that $\frac{1}{2}\Big(\frac{1}{\sqrt{1-z_{kn}^2}}+\text{Tr}(\mathbf{R}_{kn}^{\text{rad}}\tilde{\mathbf{H}}_{kn})+\sum_{j\neq k,j\in\mathcal{K}}\text{Tr}(\mathbf{R}_{jn}^{\text{off}}\tilde{\mathbf{H}}_{jn})\Big)^2$ and $\frac{1}{2}\Big(\frac{1}{1-z_{kn}^2}+\big(\text{Tr}(\mathbf{R}_{kn}^{\text{rad}}\tilde{\mathbf{H}}_{kn})+\sum_{j\neq k,j\in\mathcal{K}}\text{Tr}(\mathbf{R}_{jn}^{\text{off}}\tilde{\mathbf{H}}_{jn})\big)^2\Big)$ are convex. Thus, the right side of eq. (57) is DC.

## REFERENCES


[1] J. A. Zhang et al., "Enabling joint communication and radar sensing in mobile networks—A survey," *IEEE Commun. Surveys Tuts.*, vol. 24, no. 1, pp. 306–345, 1st Quart., 2022.

[2] Z. Yang, D. Li, N. Zhao, Z. Wu, Y. Li, and D. Niyato, "Secure precoding optimization for NOMA-aided integrated sensing and communication," *IEEE Trans. Commun.*, vol. 70, no. 12, pp. 8370–8382, Dec. 2022.

[3] M. C. Vuran, A. Salam, R. Wong, and S. Irmak, "Internet of underground things: Sensing and communications on the field for precision agriculture," in *Proc. IEEE 4th World Forum Internet Things (WF-IoT)*, Feb. 2018, pp. 586–591.

[4] F. Liu, Y.-F. Liu, A. Li, C. Masouros, and Y. C. Eldar, "Cramér–Rao bound optimization for joint radar-communication beamforming," *IEEE Trans. Signal Process.*, vol. 70, pp. 240–253, 2022.

[5] B. Liu, J. Liu, and N. Kato, "Optimal beamformer design for millimeter wave dual-functional radar-communication based V2X systems," *IEEE J. Sel. Areas Commun.*, vol. 40, no. 10, pp. 2980–2993, Oct. 2022.

[6] Z. Ni, J. A. Zhang, K. Yang, X. Huang, and T. A. Tsiftsis, "Multi-metric waveform optimization for multiple-input single-output joint communication and radar sensing," *IEEE Trans. Commun.*, vol. 70, no. 2, pp. 1276–1289, Feb. 2022.

[7] W. Yuan, Z. Wei, S. Li, J. Yuan, and D. W. K. Ng, "Integrated sensing and communication-assisted orthogonal time frequency space transmission for vehicular networks," *IEEE J. Sel. Topics Signal Process.*, vol. 15, no. 6, pp. 1515–1528, Nov. 2021.

[8] C. Dou, N. Huang, Y. Wu, L. Qian, and T. Q. S. Quek, "Sensing-efficient NOMA-aided integrated sensing and communication: A joint sensing scheduling and beamforming optimization," *IEEE Trans. Veh. Technol.*, early access, May 18, 2023, doi: 10.1109/TVT.2023.3277734.

[9] L. Chen, Z. Wang, J. Jiang, Y. Chen, and F. R. Yu, "Full-duplex SIC design and power allocation for dual-functional radar-communication systems," *IEEE Wireless Commun. Lett.*, vol. 12, no. 2, pp. 252–256, Feb. 2023.

[10] Y. Zhang, J. Chen, C. Zhong, H. Peng, and W. Lu, "Active IRS-assisted integrated sensing and communication in C-RAN," *IEEE Wireless Commun. Lett.*, vol. 12, no. 3, pp. 411–415, Mar. 2023.

[11] R. Zhang, X. Jing, S. Wu, C. Jiang, J. Mu, and F. R. Yu, "Device-free wireless sensing for human detection: The deep learning perspective," *IEEE Internet Things J.*, vol. 8, no. 4, pp. 2517–2539, Feb. 2021.

[12] Z. Zhao, M. C. Vuran, F. Guo, and S. D. Scott, "Deep-waveform: A learned OFDM receiver based on deep complex-valued convolutional networks," *IEEE J. Sel. Areas Commun.*, vol. 39, no. 8, pp. 2407–2420, Aug. 2021.

[13] H. Djigal, J. Xu, L. Liu, and Y. Zhang, "Machine and deep learning for resource allocation in multi-access edge computing: A survey," *IEEE Commun. Surveys Tuts.*, vol. 24, no. 4, pp. 2449–2494, 4th Quart., 2022.

[14] A. Asheralieva, D. Niyato, and Z. Xiong, "Auction-and-learning based Lagrange coded computing model for privacy-preserving, secure, and resilient mobile edge computing," *IEEE Trans. Mobile Comput.*, vol. 22, no. 2, pp. 744–764, Feb. 2023.

[15] Z. Yang, S. Bi, and Y. A. Zhang, "Dynamic offloading and trajectory control for UAV-enabled mobile edge computing system with energy harvesting devices," *IEEE Trans. Wireless Commun.*, vol. 21, no. 12, pp. 10515–10528, Dec. 2022.

[16] Y. Wang, Z. Su, T. H. Luan, R. Li, and K. Zhang, "Federated learning with fair incentives and robust aggregation for UAV-aided crowdsensing," *IEEE Trans. Netw. Sci. Eng.*, vol. 9, no. 5, pp. 3179–3196, Sep. 2022.

[17] X. Huang, P. Li, R. Yu, Y. Wu, K. Xie, and S. Xie, "FedParking: A federated learning based parking space estimation with parked vehicle assisted edge computing," *IEEE Trans. Veh. Technol.*, vol. 70, no. 9, pp. 9355–9368, Sep. 2021.

[18] N. Cheng et al., "Space/aerial-assisted computing offloading for IoT applications: A learning-based approach," *IEEE J. Sel. Areas Commun.*, vol. 37, no. 5, pp. 1117–1129, May 2019.

[19] L. Huang, S. Bi, and Y. A. Zhang, "Deep reinforcement learning for online computation offloading in wireless powered mobile-edge computing networks," *IEEE Trans. Mobile Comput.*, vol. 19, no. 11, pp. 2581–2593, Nov. 2020.

[20] M. S. Elbamby et al., "Wireless edge computing with latency and reliability guarantees," *Proc. IEEE*, vol. 107, no. 8, pp. 1717–1737, Aug. 2019.

[21] C. Li, C. She, N. Yang, and T. Q. S. Quek, "Secure transmission rate of short packets with queueing delay requirement," *IEEE Trans. Wireless Commun.*, vol. 21, no. 1, pp. 203–218, Jan. 2022.

[22] C. Pan, H. Ren, Y. Deng, M. Elkashlan, and A. Nallanathan, "Joint blocklength and location optimization for URLLC-enabled UAV relay systems," *IEEE Commun. Lett.*, vol. 23, no. 3, pp. 498–501, Mar. 2019.

[23] Y. Cai, X. Jiang, M. Liu, N. Zhao, Y. Chen, and X. Wang, "Resource allocation for URLLC-oriented two-way UAV relaying," *IEEE Trans. Veh. Technol.*, vol. 71, no. 3, pp. 3344–3349, Mar. 2022.

[24] Y. Zhou, F. R. Yu, J. Chen, and B. He, "Joint resource allocation for ultra-reliable and low-latency radio access networks with edge computing," *IEEE Trans. Wireless Commun.*, vol. 21, no. 1, pp. 444–460, Jan. 2022.

[25] H. Ren, C. Pan, Y. Deng, M. Elkashlan, and A. Nallanathan, "Joint pilot and payload power allocation for massive-MIMO-enabled URLLC IIoT networks," *IEEE J. Sel. Areas Commun.*, vol. 38, no. 5, pp. 816–830, May 2020.

[26] C. She, C. Liu, T. Q. S. Quek, C. Yang, and Y. Li, "Ultra-reliable and low-latency communications in unmanned aerial vehicle communication systems," *IEEE Trans. Commun.*, vol. 67, no. 5, pp. 3768–3781, May 2019.

[27] Q. Liu, H. Liang, R. Luo, and Q. Liu, "Energy-efficiency computation offloading strategy in UAV aided V2X network with integrated sensing and communication," *IEEE Open J. Commun. Soc.*, vol. 3, pp. 1337–1346, 2022.

[28] N. Huang, T. Wang, Y. Wu, Q. Wu, and T. Q. S. Quek, "Integrated sensing and communication assisted mobile edge computing: An energy-efficient design via intelligent reflecting surface," *IEEE Wireless Commun. Lett.*, vol. 11, no. 10, pp. 2085–2089, Oct. 2022.

[29] A. Farina, "Introduction to radar signal and data processing: The opportunity," Selex Sistemi Integrati, Rome, Italy, Tech. Rep. O-ENSET-063, Sep. 2006.

[30] K. Chen, Y. Wang, J. Zhao, X. Wang, and Z. Fei, "URLLC-oriented joint power control and resource allocation in UAV-assisted networks," *IEEE Internet Things J.*, vol. 8, no. 12, pp. 10103–10116, Jun. 2021.

[31] A. Ranjha and G. Kaddoum, "URLLC facilitated by mobile UAV relay and RIS: A joint design of passive beamforming, blocklength, and UAV positioning," *IEEE Internet Things J.*, vol. 8, no. 6, pp. 4618–4627, Mar. 2021.

[32] X. Liu, T. Huang, N. Shlezinger, Y. Liu, J. Zhou, and Y. C. Eldar, "Joint transmit beamforming for multiuser MIMO communications and MIMO radar," *IEEE Trans. Signal Process.*, vol. 68, pp. 3929–3944, 2020.

[33] J. Liu and M. Saquib, "Transmission design for a joint MIMO radar and MU-MIMO downlink communication system," in *Proc. IEEE Global Conf. Signal Inf. Process. (GlobalSIP)*, Nov. 2018, pp. 196–200.

[34] J. He, L. Chen, and G. Wei, "Waveform design for dual-functional radar and communication design based on conditional MI," in *Proc. 7th Int. Conf. Comput. Commun. (ICCC)*, Dec. 2021, pp. 1026–1030.

[35] B. Tang and J. Li, "Spectrally constrained MIMO radar waveform design based on mutual information," *IEEE Trans. Signal Process.*, vol. 67, no. 3, pp. 821–834, Feb. 2019.

[36] S. Bi and Y. J. Zhang, "Computation rate maximization for wireless powered mobile-edge computing with binary computation offloading," *IEEE Trans. Wireless Commun.*, vol. 17, no. 6, pp. 4177–4190, Jun. 2018.

[37] S. Boyd and L. Vandenberghe, *Convex Optimization*. Cambridge, U.K.: Cambridge Univ. Press, 2004.

[38] L. T. H. An and P. D. Tao, "The DC (difference of convex functions) programming and DCA revisited with DC models of real world nonconvex optimization problems," *Ann. Oper. Res.*, vol. 133, nos. 1–4, pp. 23–46, Jan. 2005.

[39] S. Mao et al., "Reconfigurable intelligent surface-assisted secure mobile edge computing networks," *IEEE Trans. Veh. Technol.*, vol. 71, no. 6, pp. 6647–6660, Jun. 2022.

[40] Y. Nesterov and A. Nemirovskii, *Interior-Point Polynomial Algorithms in Convex Programming*. Philadelphia, PA, USA: SIAM, 1994.

[41] W. W. Hager and H. Zhang, "A new active set algorithm for box constrained optimization," *SIAM J. Optim.*, vol. 17, no. 2, pp. 526–557, Jan. 2006.

[42] J. Müller and M. Day, "Surrogate optimization of computationally expensive black-box problems with hidden constraints," *INFORMS J. Comput.*, vol. 31, no. 4, pp. 689–702, Oct. 2019.

[43] P. T. Boggs and J. W. Tolle, "Sequential quadratic programming for large-scale nonlinear optimization," *J. Comput. Appl. Math.*, vol. 124, nos. 1–2, pp. 123–137, Dec. 2000.

[44] V. Torczon, "Pattern search methods for nonlinear optimization," *SIAG/OPT Views News*, vol. 6, pp. 7–11, Jan. 1995.

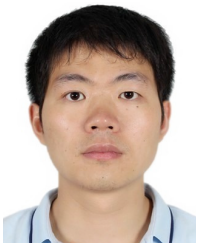

**Ning Huang** received the B.Sc. degree in electronic science and technology and the M.S. degree in optical engineering from the University of Electronic Science and Technology of China in 2009 and 2012, respectively. He is currently pursuing the Ph.D. degree with the Department of Computer and Information Science, University of Macau, Macau, China. His current research interest focuses on intelligent reflecting surface, mobile edge computing, and federated learning.

**Chenglong Dou** (Graduate Student Member, IEEE) received the B.Sc. degree in communication engineering from Jilin University, China, in 2022. He is currently pursuing the Ph.D. degree with the Department of Computer and Information Science, University of Macau, Macau, China. His current research interest focuses on mobile edge computing, non-orthogonal multiple access, and integrated sensing and communication.

**Yuan Wu** (Senior Member, IEEE) received the Ph.D. degree in electronic and computer engineering from The Hong Kong University of Science and Technology in 2010. He is currently an Associate Professor with the State Key Laboratory of Internet of Things for Smart City, University of Macau, Macau, China, where he is also with the Department of Computer and Information Science. His research interests include resource management for wireless networks, green communications and computing, edge computing and edge intelligence, and energy informatics. He received the Best Paper Award from the IEEE ICC'2016, IEEE TCGCC'2017, IWCMC'2021, and WCNC'2023. He served as the Track Co-Chair/the Symposium Co-Chair for IEEE VTC'2017-Fall, VTC'2021-Spring, VTC'2022-Spring, and ICCC'2023. He is on the editorial board of IEEE TRANSACTIONS ON VEHICULAR TECHNOLOGY, IEEE TRANSACTIONS ON NETWORK SCIENCE AND ENGINEERING, and IEEE INTERNET OF THINGS JOURNAL.

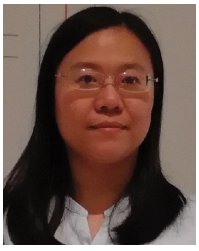

**Liping Qian** (Senior Member, IEEE) received the Ph.D. degree in information engineering from The Chinese University of Hong Kong, China, in 2010. She was a Post-Doctoral Research Associate with The Chinese University of Hong Kong, from 2010 to 2011. Since 2011, she has been with the College of Information Engineering, Zhejiang University of Technology, Hangzhou, China, where she is currently a Full Professor. From 2016 to 2017, she was a Visiting Scholar with the Broadband Communications Research Group, ECE Department, University of Waterloo. Her research interests include wireless communication and networking, resource management in wireless networks, massive IoTs, mobile edge computing, emerging multiple access techniques, and machine learning oriented toward wireless communications. She was a co-recipient of the IEEE Marconi Prize Paper Award in Wireless Communications in 2011, the Best Paper Award from IEEE ICC 2016, the Best Paper Award from IEEE Communication Society GCCTC 2017, the Best Paper Award from the Digital Communications and Networking in 2021, and the Best Paper Award from IEEE WCNC 2023. She was an Associate Editor of the *IET Communications*, from 2016 to 2022. She is on the editorial board of IEEE TRANSACTIONS ON COGNITIVE COMMUNICATIONS AND NETWORKING.

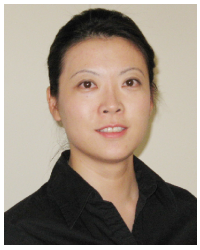

**Bin Lin** (Senior Member, IEEE) received the B.S. and M.S. degrees from Dalian Maritime University, Dalian, China, in 1999 and 2003, respectively, and the Ph.D. degree from the Broadband Communications Research Group, Department of Electrical and Computer Engineering, University of Waterloo, Waterloo, ON, Canada, in 2009. She is currently a Full Professor with the Department of Information Science and Technology, Dalian Maritime University. She was a Visiting Scholar with George Washington University, Washington, DC, USA, from 2015 to 2016. Her current research interests include wireless communications, network dimensioning and optimization, resource allocation, artificial intelligence, maritime communication networks, edge/cloud computing, wireless sensor networks, and the Internet of Things. She is an Associate Editor of *IET Communications*.

**Haibo Zhou** (Senior Member, IEEE) received the Ph.D. degree in information and communication engineering from Shanghai Jiao Tong University, Shanghai, China, in 2014. From 2014 to 2017, he was a Post-Doctoral Fellow with the Broadband Communications Research Group, Department of Electrical and Computer Engineering, University of Waterloo, Waterloo, ON, Canada. He is currently a Full Professor with the School of Electronic Science and Engineering, Nanjing University, Nanjing, China. His research interests include resource management and protocol design in B5G/6G networks, vehicular ad hoc networks, and space-air-ground-integrated networks.

He was a recipient of the 2019 IEEE ComSoc Asia–Pacific Outstanding Young Researcher Award. He served as the Track Co-Chair/the Symposium Co-Chair for IEEE/CIC ICCC 2019, IEEE VTC-Fall 2020, IEEE VTC-Fall 2021, and IEEE GLOBECOM 2022. He is an Associate Editor of IEEE TRANSACTIONS ON WIRELESS COMMUNICATIONS, IEEE INTERNET OF THINGS JOURNAL, *IEEE Network Magazine*, and IEEE WIRELESS COMMUNICATIONS LETTERS. He was selected as an IEEE ComSoc Distinguished Lecturer for the class of 2023–2024.

**Xuemin (Sherman) Shen** (Fellow, IEEE) received the Ph.D. degree in electrical engineering from Rutgers University, New Brunswick, NJ, USA, in 1990. He is a University Professor with the Department of Electrical and Computer Engineering, University of Waterloo, Canada. His research focuses on network resource management, wireless network security, the Internet of Things, 5G and beyond, and vehicular networks.

He is a registered Professional Engineer of Ontario, Canada; an Engineering Institute of Canada Fellow; a Canadian Academy of Engineering Fellow; a Royal Society of Canada Fellow; a Chinese Academy of Engineering Foreign Member; and a Distinguished Lecturer of the IEEE Vehicular Technology Society and Communications Society. He received the "West Lake Friendship Award" from Zhejiang Province in 2023, the President's Excellence in Research from the University of Waterloo in 2022, the Canadian Award for Telecommunications Research from the Canadian Society of Information Theory (CSIT) in 2021, the R. A. Fessenden Award in 2019 from IEEE Canada, the Award of Merit from the Federation of Chinese Canadian Professionals (Ontario) in 2019, the James Evans Avant Garde Award from the IEEE Vehicular Technology Society in 2018, the Joseph LoCicero Award in 2015, the Education Award from the IEEE Communications Society (ComSoc) in 2017, and the Technical Recognition Award from the Wireless Communications Technical Committee in 2019 and the AHSN Technical Committee in 2013. He has also received the Excellent Graduate Supervision Award from the University of Waterloo in 2006; and the Premier's Research Excellence Award (PREA) from the Province of Ontario, Canada, in 2003. He serves/served as the General Chair for the 6G Global Conference'2023 and ACM Mobihoc'2015; the Technical Program Committee Chair/the Co-Chair for IEEE Globecom'2024, 2016, and 2007, IEEE Infocom'2014, IEEE VTC'2010 Fall; and the Chair for the IEEE ComSoc Technical Committee on Wireless Communications. He is the President of the IEEE ComSoc. He was the Vice President for Technical and Educational Activities, the Vice President for Publications, the Member-at-Large on the Board of Governors, the Chair of the Distinguished Lecturer Selection Committee, and a member of IEEE Fellow Selection Committee of the ComSoc. He served as the Editor-in-Chief for the IEEE INTERNET OF THINGS JOURNAL, IEEE NETWORKS, and *PPNA*.